中图分类号：TH133.3 论文编号：10287
0511-0228
学科分类号：080203

硕士学位论文

磁悬浮轴承金属橡胶环组合支承性能参数优化

研究生姓名 **Uzoma Gregory Okoro**
学科、专业 机械设计及理论
研 究 方 向 机电一体化
指 导 教 师 谢振宇 副教授
郭勤涛 副教授

南京航空航天大学
研究生院 机电学院

二O一一年一月

Nanjing University of Aeronautics and Astronautics
The Graduate School
College of Mechanical and Electrical Engineering

Complexed Active Magnetic Bearing Metal Rubber Ring Performance Parameters Optimization

A Thesis in

Mechanical Design and Theory

By

Uzoma Gregory Okoro

Advised by

Associate Professor Xie Zhenyu and Guo Qintao

Submitted in Partial Fulfillment

Of the Requirements

For the Degree of

Master of Engineering

January, 2011

承诺书

本人声明所呈交的硕士学位论文是本人在导师指导下进行的研究工作及取得的研究成果。除了文中特别加以标注和致谢的地方外，论文中不包含其他人已经发表或撰写过的研究成果，也不包含为获得南京航空航天大学或其他教育机构的学位或证书而使用过的材料。

本人授权南京航空航天大学可以将学位论文的全部或部分内容编入有关数据库进行检索，可以采用影印、缩印或扫描等复制手段保存、汇编学位论文。

(保密的学位论文在解密后适用本承诺书)

作者签名：_____

日　　期：_____

ABSTRACT

To reduce the vibration of flexible rotor supported on Active Magnetic Bearing (AMB), Metal Rubber Ring (MRR) is introduced and set around the AMB, hereafter called Complex Bearing (CB). Dynamic characteristics and Parameters Optimization of the system supported by CBs are studied in this thesis by theoretical analysis, Experimental Modal Analysis (EMA) and actual operation of the system. The main contents are as follows:

1) Presentation of the components and working principle of the CB-rotor system, highlighting structure of the CB.
2) Analysis of demonstrative bearing-rotor system has been carried out to guarantee the whole modeling and analysis of the system is valid. The mathematic model of Free-Free rotor and CB are individually established in Patran and their natrual frequencies calculated by MD-Nastran.
3) The mathematic model of CB-rotor system is also established and natural frequencies, modal damping, unbalance response and influence of CB performance parameters on dynamic characteristics of the system are investigated.
4) An optimization method is adopted and a case study with four design variables was conducted by using Nastran solution 200.
5) Dynamic characteristics of the CB-rotor system are investigated by EMA and actual operation of the system.

The research results show that the first four modal damping ratios of the CB-rotor system are heavy and the system can get across the first two bending critical speeds safely.

Keywords: AMB; MRR; Modal Parameter; Sensitivity Analysis; Optimization

CONTENT

LIST OF FIGURES AND TABLES

NOMENCLATURE

A_a	area of air gap	ρ	density
C	damping	μ_n	unit length
c_{a}	AMB damping	γ_n	element displacement angle
D	damping matrix	n	beam element
E	youngs modulus	μ_0	permeability of air
e_n	mass eccentricity	Ω	excitation frequency
$F(i,x)$	bearing force	ω	rotation frequency
G	gyroscopic matrice		
$G_{\mathrm{c}}(s)$	controller tranfer function		
$G_{\mathrm{p}}(s)$	amplfier tranfer function		
$G_{\mathrm{s}}(s)$	sensor tranfer function		
i_0	bias current		
i_x	control current		
J_p	polar moment of inertia		
J_d	diametral moment of inertia		
K	stiffness matrix		
K_d	derivative coefficient		
K_i	integeral coefficient		
K_p	propotional coefficient,		
k_i	current stiffness		
k_s	position stiffness		
L	inductor		
M	mass matrix		
N	number of turns of coil		
T_n,	transformation matrice		
U	control signal		
x	air gap.		

Chapter 1 Introduction

1.1 Historical Review and State of the Art

Active Magnetic Bearing (AMB) is a mechatronic product.Its mechanical and electrical parts interact suitably to yield variable magnetic force capable of keeping a levitated body in intended position stably regardless of the external disturbances. AMB has enviable qualities, such as active control, contactless support, clean operating environment etc. These raised interest in researches on it's applicability in industries [1].

In 1842, British physicist S. Earnshaw proposed the concept of magnetic suspension. He proved theoretically that it was impossible to suspend an object stably in all six degrees of freedom just by action of permanent magnet alone[2]. In 1937, Kemper suggested that continuous adjustment of magnetic force through controllable electromagnet is the solution to unstable suspension [3]. It became the dominant idea of magnetic technology research.

Modern magnetic technology began in 1957 with the proposal by Hispano-Suiza (French company) to use electromagnet and inductive sensor to compose active suspension system. This latter yielded the French patent. In 1969, the French army research laboratory used magnetic bearing to support satellite guide wheel. After that magnetic bearing found way into defense and aerospace fields. With the development of modern control theory, electronic, computer technologies and materials between late 70's to early 80's, AMB finally found applications in industrial equipment. The corresponding control method was developed from, Single-input and single-output (SISO Classical Control Theory) to Multi-input and multi-output (MIMO Modern Control Theory). With the development of high speed and light weight machines in early 90's, it became evident that rigid rotors can no longer meet the actual demand, prompting researchers to start research on flexible rotor system supported by AMB [4].

A large number of researches on magnetic bearing have been carried out and some products were brought into the industrial application. There are some famous research institutions and companies involved in these researches. Amongst them are: Virginia University, University of Maryland, Berkeley University, University of Texas at Austin, NASA, Tokyo University, Chiba University, SEIKO, MECOS company of Switzerland, REVOLVE company of Canada, S2M company of France, etc. Since 1988, the International Symposium on Magnetic Bearings (ISMB) had been held bianually.

1.2 Research Background

AMBs, despite all the advantages, cannot be effectively applied into the actual flexible rotor system because the supporting damp is too light that the vibration of the rotor is not easy to be restrained especially when the system operates near or over the bending critical speeds. On the other hand, so-called non-collocation problem of sensor and electromagnet in radial AMB usually occurs due to limited space around the rotor and then it is always true that at least one undamped flexible mode shape will exhibit a node between a sensor-actuator pair. If this mode has a frequency within the bandwidth of the controller, then it poses special dynamics problems for the system. Both of these issues must be addressed either explicitly or implicitly in the design of AMB controller for a flexible rotor[5].

So far, two methods are adopted to solve the above problems; modern control strategies and unbalance compensation. Decoupling vibration control approach for a flexible rotor system with symmetric mass and stiffness matrices was studied in [7]. In [8], reported case of an active control procedure for flexible rotors supported by magnetic bearings was presented. There controller however failed when gyroscopic effects were considered. In [9], an approach that designed a dedicate feedback control to completely remove the gyroscopic effects was proposed, which then makes decoupling of the governing equations possible. However, as reported in [10], the gyroscopic effects may serve to improve the system behaviour with large external damping. Pole placement techniques for synchronous vibration control of AMB-rotor system was reported in [11], while [12] conducted experiments on unbalance control of such system using adaptive control techniques. Detailed description of the electromagnetic actuator for active vibration control of a flexible rotor was presented in [13], and the synchronous vibrations of a rotor system were greatly reduced by the proposed algorithm based on the least-squares method. Report of design of feedback gain controller using PID and LQ control laws to control the rigid and flexible modes respectively of rotor-AMB system was presented in [14]. In the same vane, [15] achieved stable rotation up to speed of 10,000 rpm with PID-stabilized flexible rotor by using LQG controller with modal weighting to suppress resonance. In a related case, [16] demonstrated, in test, that the dual usage of Analog Control plus Phase Bump Filter (PBF) could control high frequency vibration through 1.5 kHz. A model-based LQ controller with an optimal observer-based unbalance force rejection control was used in [17] to lower the vibration amplitude of a variable speed magnetically suspended rotor.

These approaches, though improved the AMB flexible rotor system, had result to too complicate a control strategies that could prove unoperable to foremen in industries.

1.3 Motivation, Objectives and Methods

It has been verified that combined support is better than single support in restraining rotor vibration. Hamburg first pointed out that vibration of rotor would be restrained effectively when ball bearing is fixed on elastic foundation[18]. Squeeze film damper (SFD) was also used to improve the performance of the Chinook helicopter drive supported by ball bearing [19].

Metal Rubber (MR) is a new kind of material that has combine characteristics of selected metal (high and low temperature resistance, corrosion resistance) and flexibility of rubber with damping ratio of about 0.35[23]. The frequency dependent excitation forces acting on the MR generates heat partly due to compression and relaxation action of the MR element and partly due to friction on contact with other elements. The heat energy is then dissipated reducing the overall energy content of the system.

Enlightened by the idea of combined support, our research team put forward a new combined support which is called Complexed Bearing (CB). CB comprises of Metal Rubber Ring (MRR) and AMB. MRR is carefully padded around AMB to increase the support flexibility. Our previous research on CB showed that MRR could increase the first bending modal damping of the system remarkably, but the parameters of AMB and MRR were not optimal[24].

AMB and MRR elements can be modeled as spring and damper. The overall bearing property becomes a function of individual properties of the bearing elements, and varying these properties results to varied rotor response. The purpose of this thesis is to find the parameter combination of AMB and MRR for the best dynamic response.

Frequency Response (FR) analysis of the system is performed by Finite Element Method (FEM) using MD Nastran and Patran. We are well informed that the most reliable way of obtaining accurate dynamic model describing the behavior of machines is through experimental procedure as it better reflects reality[25]. For that purpose, we will perform Experimental Modal Analysis (EMA) and actual operations of the system and used the result to validate the FEM model.

1.4 Structure of the Thesis

In chapter 2, the components of CB-rotor System are highlighted. The whole assemble is presented and the working principle of the system is explained with aids of detailed diagrams.

In Chapter 3 The analysis tool, Nastran is introduced and used to perform Whirl frequency analysis, Critical speed as well as Unbalanced response analysis of the CB- rotor system.

In chapter 4 Finite Element Sensitivity-based Optimization method for the CB-rotor system was

illustrated. Aiming at obtaining high damping ratios within the regions of bending critical speeds, a case study with five design variables was conducted using Nastran solution 200.

Chapter 5 discusses tests. It begins with EMA and the ends with actual operation of the system. The descriptions of the test procedures are well outlined and the apparatus used for the various tests carefully identified.

In chapter 6, main work and conclusions are presented and further research work which could be made for more effective optimization are mentioned.

Chapter 2 Basic Component of CB-Rotor System

The system comprises of two units: Mechanical and Electronic unit. The Mechanical Unit consists of Rotor and CB subsystems.The CB itself has the AMB and MRR.

The Electronic Unit include: Sensor, Controller and Power Amplifier.We will go ahead and explore definitions and features of these components. Most of the facts are extracted from [26].

2.1 Sensor

Sensors are used to dictate the movement of the rotor. Several sensor types are used in AMBs: inductive, eddy current, capacity and optical displacement sensors. Each has advantages in specific applications, but the general properties that need to be assessed are: Bandwidth, Electrical noise and Magnetic field rejection, Robustness to environment, Compatibility to canning in harsh service environments, Reliability, Cost [27]

Since AMBs are actively controlled regarding to the sensor signal, the control performance strongly depends on the sensor performance.

In this study eddy current sensor is utilized. It used the principle of electromagnetism: as the rotor approaches the sensor, the electromagnet field surrounding the sensor becomes stronger.

The sensor transfer function is given by:

$$G_s(s) = \frac{\text{Gain} \cdot \omega_{BW}}{s + \omega_{BW}} (\text{V/m}) \tag{2.1}$$

where ω_{BW} is the sensor bandwidth frequency.

2.2 Controller

The controller has its input as the rotor motion (may include the velocity and phase) and out puts voltage to the actuator. It processes the input signal through a carefully designed algorithm to determine the output signal-voltage. Mordern AMB systems nearly always use digital controllers. These controllers are described in terms of their:

(1) Sampling rate .i.e. the frequency of measurement of the sensor signal and update the amplifier signal.

(2) Delay i.e. time elapse between measurement as well as processing time.

(3) Algorithm.

The controller can be described in terms of frequency domain transfer functions within $G_c(s)$:

$$\{V_c\} = [G_c(s)]\{V_s\} \tag{2.2}$$

where, V_c is output voltage of controller, V_s is output voltage of sensor, and $G_c(s)$ is transfer function of controller,

$$G_c(s) = \begin{matrix} G_c(s)_{1,1} & \text{L} & G_c(s)_{1,n} \\ \text{M} & \text{O} & \text{M} \\ G_c(s)_{n,1} & \text{L} & G_c(s)_{n,n} \end{matrix} \tag{2.3}$$

The classic Proportional-Integral-Derivative (PID) algorithm is a common place to start when designing an AMB control system. A typical PID frequency response is written as:

$$G_{\text{PID}}(s) = (K_p + \frac{K_i}{s} + K_d s)(\frac{\omega_{BW}^2}{s^2 + 2\xi\omega_{BW}s + \omega_{BW}^2}) \ \text{(V/V)} \tag{2.4}$$

where, K_p is propotional coefficient, K_i is integeral coefficient, and K_d is derivative coefficient.

2.3 Power Amplifier

Current is induced in the coils of the electromagnets by power amplifiers. These amplifiers are designed to apply large voltages to the coils and to monitor resulting currents. The currents are typically compared to a request signal (provided by the AMB controller) and the voltage adjusts to try to force the current assume the request value –transconductance[28]. In understanding the behavior of AMB, it is petinent to recorgnise that the power amplifier can only apply a finite voltage, fixed by the power supply (V_{max}) and that this limits how rapidly the AMB force can vary because of electromagnetic inductance. If the coil set driven by a power amplifier has inductance L and resistance R, then the coil voltage (applied by the power amplifier) is related to the coil current by:

$$V = RI + L\frac{di}{dt} + I\frac{dl}{dt} \tag{2.5}$$

The power amplifier is characterized by its gain, bandwidth, voltage limit, and maximum current. For a given electromagnetic set, the maximum current I_{max} should be matched to the saturation current for the electromagnets I_{sat}. Then the dynamic capacity of the AMB given above will be controlled by the maximum amplifier voltage (V_{max}) and the ratio between bias current and maximum control current.

The Amplifier frequency response characteristics, the transfer function, is given by

$$G_{\mathrm{AMP}}(s)=\frac{\mathrm{Gain}\cdot\omega_{\mathrm{BW}}^2}{s^2+2\xi\omega_{\mathrm{BW}}s+\omega_{\mathrm{BW}}^2}\ \ (\mathrm{A/V}) \tag{2.6}$$

2.4 Rotor

By rotor, we mean "shaft" and shrunk-on components like sleeves, varying cross-section area, impellers/bladed disks etc. The rotor is designed to meet required mechanical properties of rigidity, stiffness, resistance to corrosion etc.

Figure 2.1 shows the schematic illustration of the rotor. Table 2.1 and 2.2 show the technical description and mass and inertia properties.

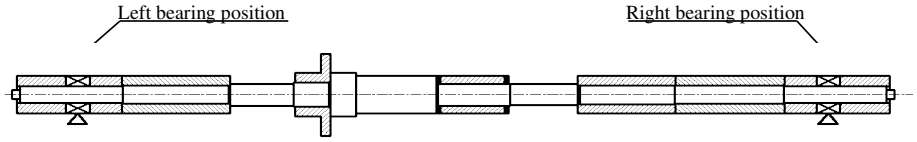

Figure 2.1 Schematic illustration of the rotor

Table 2.1 Size parameters of the rotor

Description	Value(mm)
Left end to right end length, L	828
Bearing center to center, l $(l=l_a+l_b)$	704
Left end to the rotor center of mass, l_c	416.4
Left bearing center to rotor center of mass, l_a	355.4
Right bearing center to rotor center of mass, l_b	348.6

Table 2.2 Rotor mass and inertia properties

Description	Value
Mass, m	$7.5322\,\mathrm{kg}$
Polar Moment of inertia, J_{p}	$0.0032\,\mathrm{kg\cdot m^2}$
Diametral Moment of inertia, J_{d}	$0.4624\,\mathrm{kg\cdot m^2}$

2.5 AMB

The AMB with the activities of the controller generates force to suspend the rotor stabily and control its motion. It is called “active” because it can respond to change in position of the rotor.

Two kinds of AMB can be identified depending on the direction of motion of the rotor they are used to control. They are: Radial AMB and Axial AMB.

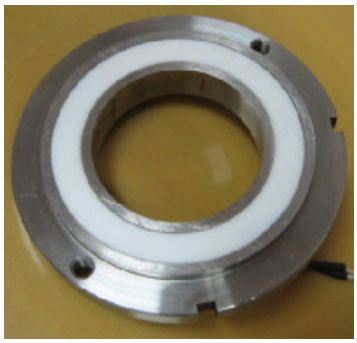

Figure 2.2 Axial or thrust AMB

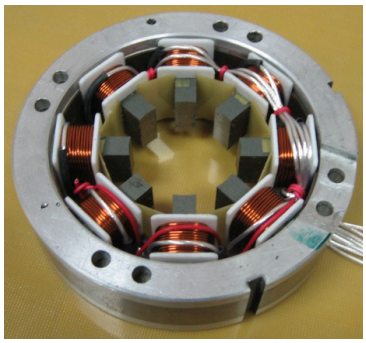

Figure 2.3 Radial AMB

Figures 2.2 and 2.3 are the pictures of AMB designed by our research team.

The main components of the AMB are; laminated iron core and the copper windings. Both constitute the bearing electromagment which together with the amplifier is called the Actuator. In addition, there is a network of wire to supply the actuating current. The iron core is laminated to reduce the effect of eddy current. High conducting material is required for the winding.

Table 2.3 Radial AMB design properties

Description	Specification
Bearing load	80.0N
Bore diameter	40.0mm
Bearing width	20.0mm
Number of turns	33.0turns
Bias current	2.5A
Clearance	0.25mm
Displacement Stiffness-coefficient.	-3.2×10^{5} N / m
Current Stiffness-coefficient	32N/A

2.6 Metal Rubber

MR materials are made of pressed stainless steel wire of diameter range of 0.1-0.5mm having both loose and reticulate structures. They have dual qualities of rubber and metal, thus the name. The metal-rubber is tight-fitted onto the periphery of the AMB base to form a single unit of CB. The picture of the AMB designed by our research laboratory is shown in Figures 2.4 and 2.5 below.

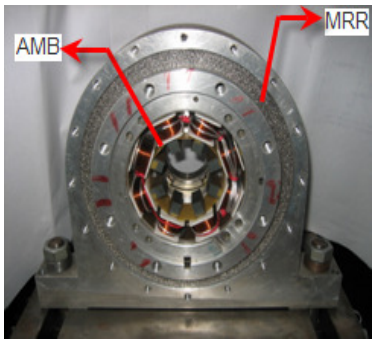

Figure 2.4 Complexed Bearing Unit

Figure 2.5 Metal Rubber Ring

2.7 CB-Rotor System

The Test CB-Rotor system is shown inFigure 2.6. Figure 2.7 shows the schematic diagram of the same system. The Rotor, driven by a high-power electric motor runs in a pre-determined position.

The motion is controlled by joint actions of two Radial CB units (Rad 1 and Rad 2) and Thrust AMB. The Radial CB controls the radial motion while the axial motion of the rotor is controlled by the action of the Thrust AMB. Sensors are placed close to actuator and rotor to detect motions of the rotor.

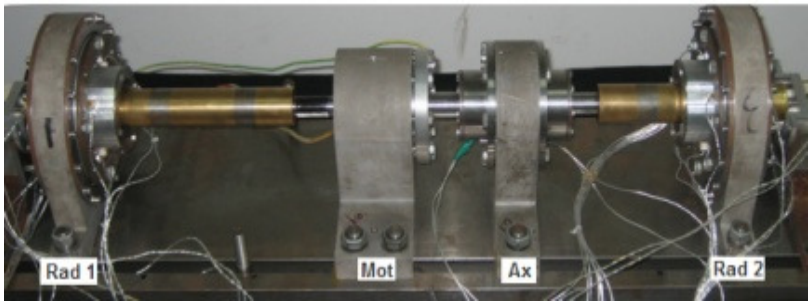

Figure 2.6 CB-rotor system

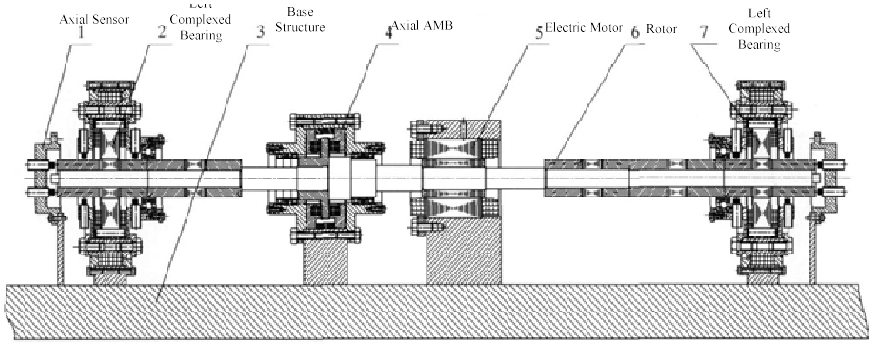

Figure 2.7 Schematic diagram of Complexed Bearing-rotor system

2.8 Working Principle

The Sensor picks the Displacement *x* of the supported rotor, and sends it to the Controller. The Controller processes the information and generates appropriate Control signal V. The position signal is transformed by the Power amplifier into Control current in the coil. The control current generates magnetic field in the actuating magnets, resulting in magnetic force in such away that the rotor remains in it hovering state. The control law of the feedback is responsible for the stability of the hovering as well as the stiffness and damping of such a suspension. Stiffness and damping can be varied within physical limit and can be adjusted to technical requirement.

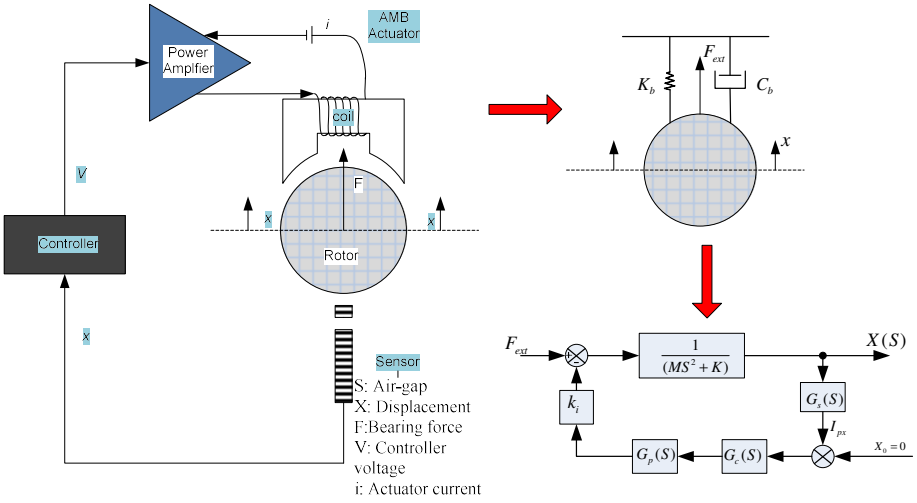

Figure 2.8 AMB principle of operation

For a pair of magnets, the force F_x [N] represents the force difference between the positive and the negative directions and is given by

$$F^+ = k\frac{(i_0 + i_x)^2}{(s_0 - x)^2} \tag{2.7}$$

$$F^- = k\frac{(i_0 - i_x)^2}{(s_0 + x)^2} \tag{2.8}$$

So that the resultant force on a single axis is

$$F = \sum F^+ - F^- = k\left(\frac{(i_o + i_x)^2}{(s_o - x_x)^2} - \frac{(i_o - i_x)^2}{(s_o + x_x)^2}\right)\cos\alpha \tag{2.9}$$

or

$$F_x = k_i i_x + k_s x \tag{2.10}$$

Where, $i_0[\mathrm{A}]$ is bias current, $i_x[\mathrm{A}]$ is control current, $s_0[\mathrm{m}]$ is nominal air gap, $x[\mathrm{m}]$ is air gaps, $k = \mu_0 N^2 A_a / 4$, N is number of turns, A_a is area of air gap, μ_0 is permeability of air, $\mu_0 = 4\pi \times 10^{-7}[\mathrm{H/m}]$ and α is the angle between the force direction and the middle of the actuator teeth (For eight actuator teeth, $\alpha = 22.5°$).

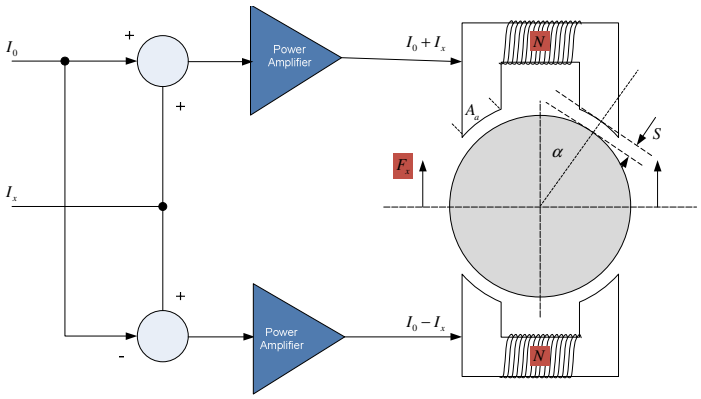

Figure 2.9 Force-Current relationship

As most simple approach, one might set up the desired control force *F* in such a way that the closed-loop behavior becomes similar to that of a mechanical spring-damper system. This results in an expression for the bearing force *F* with linear coefficients for equivalent stiffness, *k* and damping, *c*[29]:

$$F = -k_{eq}x - c_{eq}x \tag{2.11}$$

where the frequency dependent k_{eq} and c_{eq} is given by

$$k_{eq}(\omega) = k_s + k_i \,\mathrm{Re}[G(j\omega)] \tag{2.12}$$

$$c_{eq}(\omega) = k_i \frac{\mathrm{Im}[G(j\omega)]}{\omega} \tag{2.13}$$

(see Figure 2.8). The transfer function is giving by the expression,

$$G(j\omega) = \frac{Y(s)}{F_{ext}} = \frac{1}{ms^2 + k_s + k_i G_s(s) G_c(s) G_{AMP}(s)} \tag{2.14}$$

2.9 Chapter Summary

This chapter is an introduction to AMB technology. The chapter discusses the components of CB, fundamental characteristics and working principle of the system. MRR characteristics are further discussed in details. The chapter ended with the description of whole CB-Rotor structure.

Chapter 3 Modeling and Dynamic Analysis of CB-Rotor System

3.1 Introduction

The dynamic response of a rotor-bearing system can be approximated by the set of linear differential equations obtained from the finite element representation. The system parameters including the geometry of the system, coefficients of bearing, inertia properties of rigid disk, and the distribution of the mass and stiffness of rotating assemblies all of which have significant influence on the dynamic characteristics of the rotor-bearing system. The representation of the shaft element as a series of beam elements is common in the application of the finite element method to rotor-bearing systems. Under a small deflection assumption, the linearized equation of motion for the shaft element can be used to model the shaft.

The rotor considered in this work is flexible and has complex geometry. Thus the use of approximate models becomes imperative.

At any time, t the radial displacement of the rotor relative to static deflection line is considered to be $x(z,t)$ and $y(z,t)$. The diagram of the discretized flexible rotor is shown in Figure 3.1 below.

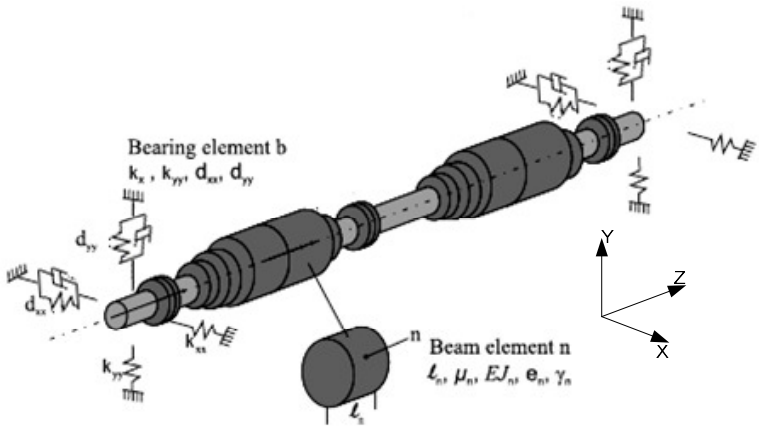

Figure 3.1 Finite Element Model of the flexible rotor system

The flexible rotor is divided into a discrete number of elements, n where each node usually is

described by two translational and two rotational degrees of freedoms (DOF). The axial translational and rotational DOF are considered fixed.

Each of these discrete models has the following properties; length l_n, bending stiffness EJ_n, mass per unit length μ_n, mass eccentricity e_n and angle of eccentricity γ_n as well as other parameters describing external and internal damping, additional inertia effect like the rotatory inertia and gyroscopic effects and self excitation mechanism.

3.1.1 Equation of Motion (EOM)

The equations of motion of a single element may be obtained by, for example from the law of conservation of momentum or Langrange's equation and analysis can be done using transfer matrix method [30], FE Method [31, 32] and Lumped Parameter mothod. Nowadays, it is a common practice to use combinations of methods: as in FE method and Modal analysis, to obtain the stiffness matrix and the inertia matrice.

We consider the virtual work of a beam element, n with unknown displacement function $x_n(z_n,t_n)$ and $y_n(z_n,t_n)$. The function can be expressed as an approximate function which has to fulfill special compatibility conditions within an element and at the boundaries. These approximations are; boundary displacement and selected deformation function for the inner area of the element. Figure 3.2 below shows the four approximate deformation functions H_1, H_2, H_3, H_4 with the corresponding boundary displacements and angle for the *y* direction.

$$x_n(z_n,t) = H_n^T X_n \tag{3.1}$$

$$y_n(z_n,t) = H_n^T Y_n \tag{3.2}$$

$$X_n^T = \{x_n^l, \beta_n^l, x_n^r, \beta_n^r\} \tag{3.3}$$

$$Y_n^T = \{y_n^l, \alpha_n^l, y_n^r, \alpha_n^r\} \tag{3.4}$$

$$H_n^T = \{H_1, H_2, H_3, H_4\} x_n \tag{3.5}$$

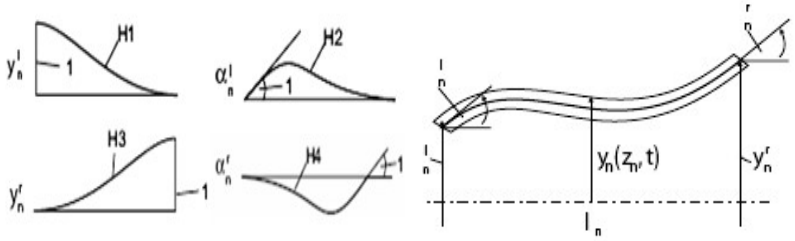

Figure 3.2 Approximate functions for element *n*

The stiffness and mass matrices of the *nth* element can be derived by applying principle of virtual work, and written as,

$$k_n = \frac{EJ_n}{l_n^3}\begin{bmatrix} 12 & 6l_n & -12 & 6l_n \\ & 4l_n^2 & -6l_n & 2l_n^2 \\ & & 12 & -6l_n \\ & & & 4l_n^2 \end{bmatrix} \tag{3.6}$$

$$m_n = \frac{\mu_n l_n}{420}\begin{bmatrix} 156 & 22l_n & 54 & -13l_n \\ & 4l_n^2 & 13l_n & -3l_n \\ & & 156 & -22l_n \\ & & & 4l_n^2 \end{bmatrix} \tag{3.7}$$

The matrices are related to the boundary forces (moments) and displacement (angle) for the element *n*. for each nodal point marking the boundary of element, *n*, four global coordinates: 2 translation and 2 rotation are define.

We concentrate all the global coordinate to one general global vector *X* (*x*-plane only) so that we can represent local element coordinate X_n as a function of global coordinates as follows

beam element $$X_n = T_n X \tag{3.8}$$

bearing element $$X_b = T_b X \tag{3.9}$$

In the above expression, T_n, T_b are transformation matrices showing how the beam and bearing elements are arranged in the overall coordinate system.

The mass, damping, stiffness matrices and the unbalance excitation vector for the whole system along x-axis written in terms of overall coordinate system is shown below

$$M_x = \sum_{n=1}^{N} T_n^T M_n T_n \tag{3.10}$$

$$D_x = \sum_{b=1}^{B} T_b^T T_b d_{bxx} \tag{3.11}$$

$$K_x = \sum_{n=1}^{N} T_n^T M_n T_n + \sum_{b=1}^{B} T_b^T T_b c_{bxx} \tag{3.12}$$

$$f_x = \sum_{n=1}^{N} T_n^T f_{ne} \tag{3.13}$$

Based on principle of virtual work, the EOM is written as

$$M_x \ddot{X} + D_x \dot{X} + K_x X = f_x \tag{3.14}$$

$$M_y \ddot{Y} + D_y \dot{Y} + K_y Y = f_y \tag{3.15}$$

for the *x* and *y* directions shown in equation 3.14 and 3.15. Assuming isotropy of elements (beam and bearing) properties, both equations are equal. For anisotropy of beam stiffness and bearing element coefficients K_y and D_y will differ along the main diagonal.

Superposing equation 3.14 and 3.15, we obtain

$$\begin{pmatrix} M_x & 0 \\ 0 & M_y \end{pmatrix} \begin{bmatrix} \ddot{X} \\ \ddot{Y} \end{bmatrix} + \begin{pmatrix} D_x & 0 \\ 0 & D_y \end{pmatrix} \begin{bmatrix} \dot{X} \\ \dot{Y} \end{bmatrix} + \begin{pmatrix} K_x & 0 \\ 0 & K_y \end{pmatrix} \begin{bmatrix} X \\ Y \end{bmatrix} = \begin{bmatrix} f_x \\ f_y \end{bmatrix} \tag{3.16}$$

For coupling, equation 3.24 can be rewritten as

$$\begin{pmatrix} M_x & M_{xy} \\ M_{yx} & M_y \end{pmatrix} \begin{bmatrix} \ddot{X} \\ \ddot{Y} \end{bmatrix} + \begin{pmatrix} D_x & D_{xy} \\ D_{yx} & D_y \end{pmatrix} \begin{bmatrix} \dot{X} \\ \dot{Y} \end{bmatrix} + \begin{pmatrix} K_x & K_{xy} \\ K_{yx} & K_y \end{pmatrix} \begin{bmatrix} X \\ Y \end{bmatrix} = \begin{bmatrix} f_x \\ f_y \end{bmatrix} \tag{3.17}$$

Coupling can result due to effect like gyroscopic moments, steam excitation, internal damping etc.

These equations can simply be written in the form

$$M\ddot{z} + D\dot{z} + Kz = f \tag{3.18}$$

where

$$z = \begin{bmatrix} x \\ y \end{bmatrix} \tag{3.19}$$

M is symmetric mass matrices ($M_{xy} = M_{yx} = 0$) and consist of the translatory and rotatory inertia terms from beam and disc elements; *D*-Damping matrix has symmetric component for external and internal damping and may contain unsymmetrical gyroscopic terms. Gyroscopic moments of beam element and most importantly from discs with high moment of inertia result in skew-symmetric matrix i.e. $G = -G^T$; Stiffness Matrix *K* consist mainly of symmetric matrix part of the beam elements Additional skew symmetrical matrix have their origin from internal damping and steam excitation. Gyroscopic moment have an effect on the natural frequencies of the rotor.

3.1.2 FEM Analysis in MD Nastran

The rotor-bearing system of modern rotating machines constitutes a complex dynamic system. Analysis procedure of rotordynamics in MD Nastran and Patran is shown as Figure 3.3. MD Nastran rotor dynamics product module provides a simple, fast and reliable method to performing the various analyses associated with rotor-bearing systems and other rotating components.

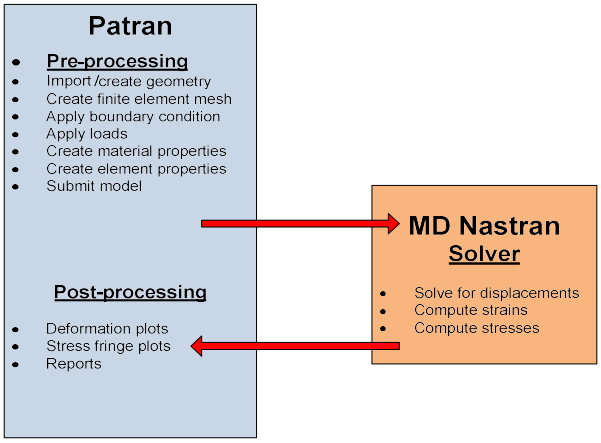

Figure 3.3 Analysis flow in MD-Nastran and Patran

Analysis of rotor in MD Nastran and Patran involve three main operations; Pre-processing, Processing and Post-Processing operations. In the pre-processing operation, the standard scalar 2-D line elements available in Patran interface is utilized in modeling the rotor. The analysis solution sequences for the processing operation includes; Sol-107 which performs complex mode analysis with asynchronous option (for the whirl modes and frequencies) and synchronous option (for the Critical speed). The analysis supported by MD Nastran includes：

1) Frequency Response Analysis (FRA): i.e. the Steady state response analysis due to unbalance and other forms of excitations.
2) Linear and Non-Linear transient response analysis: to determine the response of the rotor system to imbalance during start-up.
3) Stability Analysis.

The result of the analysis is then sent back to Patran to perfom the Post-processing operation, which mainly has to do with result(s) processing through XDB files and visualizing the deformation plots and stress fringe plots and can be presented in the forms of reports.

The MSC Nastran time and frequency-domain equation solved by the dynamic solution sequences is;

$$M\ddot{u}(t)+\left(B_s+\left(\frac{g}{W3}\right)K_s+\left(\frac{1}{W4}\right)K4_s+B_r+\left(\frac{gr}{WR3}\right)K_r+\left(\frac{1}{WR4}\right)K4_r+\Omega B^G\right)\dot{Z}(t)$$
$$+\left(K_s+K_r\Omega\left(K^{cv}+\left(\frac{g_r}{WR3}\right)K^{Cgr}+\left(\frac{1}{WR4}\right)K^{Cge}\right)\right)z(t)=F(\omega) \tag{3.28}$$

$$\left(\begin{array}{l}-\omega^2M+i\omega(B_s+B_r+\Omega B^G)\\ \quad+\left(\begin{array}{l}(1+ig)K_s+iK4_s+(1+ig_r)K_ri\\ +K4_r\Omega\left(K^{Cv}+\left(\frac{gr}{\omega}\right)K^{Cgr}+\left(\frac{1}{\omega}\right)K^{Cge}\right)\end{array}\right)\end{array}\right)u(\omega)=F(\omega) \tag{3.29}$$

where,

M is total mass matrix (CONMi, CMASSi, MATi)

B_s — support viscous dampimg matrix (CVISC, CDAMPi)

$\left(\frac{g}{W3}\right)K_s$ —support viscous damping equivalent to structural damping (PARAM,G)

$\left(\frac{1}{W4}\right)K4_s$ —support viscous damping equivalent to material structural Damping (GE on MATi)

B_r —rotor viscous damping matrix (CVISC, CDAMPi)

$\left(\frac{gr}{WR3}\right)K_r$ —rotor viscous damping equivalent to structural damping (GR on RSPINT)

$\left(\frac{1}{WR4}\right)K4_r$ —rotor viscous damping equivalent to material structural damping (GE on MATi)

B^G —gyroscopic force matrix (dependent on polar moment of inertia)

K_s —support stiffness matrix

K_r —rotor stiffness matrix

$K4_s$ —support material damping matrix (GE on MATi)

$K4_r$ —rotor material damping matrix (GE on MATi)

Ω —rotor spin rate

K^{Cv} —“circulation” matrix due to B_r

$g_r K_r^{Cgr}$ — "circulation" matrix due to $g_r K_r$

K_r^{Cge} —"circulation" matrix due to $K4_r$

ω —whirl frequency

G, *WR3*, *WR4* are user parameters

SOL 107 (direct method) solves the critical speed using SYNC card. Here it substitutes $\omega = \Omega$ in Equation 3.29. The resulting Equation 3.30 is solved for Ω:

$$\begin{pmatrix} -\Omega^2 (M - iB^G) + i\Omega\left(B_s + B_r - iK^{Cv}\right) \\ + \left(1 + ig\right) K_s + iK4_s + (1 + ig_r) K_r i \\ + iK4_r g_r K^{Cgr} + K^{Cge} \end{pmatrix} u(\Omega) = F(\Omega) \qquad (3.30)$$

Critical speeds can also be determined by the whirl frequency calculation, using the Campbell. Campbell diagram plots the eigenvalue versus the rotor speed. Eigenvalues with similar mode shapes are connected to form a series of line that represent changing natural frequencies. Critical speeds are determined by assessing which eigenvalues are identical to the rotor speed. This is done by drawing line $\omega = \Omega$, natural frequency = rotor spin). The intersection of this line with the eigenvalue lines ($1\times$ revolution line) are the critical speeds.

3.1.3 Demonstrative Example

a) MODEL: The rotor is modeled as 8 rigid beam elements connected at nodes. The disc is located at the 7th grid point. The concentrated masses of the beams and disc are modeled as lumped masses. The rotor ends are attached to the support bearings through Rigid Body Element (RBE) 2 element. This is to ensure separation of the mass damping or stiffness of the rotor from that of the bearing or support structure. The bearing itself is modeled using CELAS1 (grounded spring) elements and connects to the ground. Connections of the rotor to the ground or support element may cause incorrect determination of the gyroscopic terms. The rotor considered in this example is shown in Figure 3.4 below.

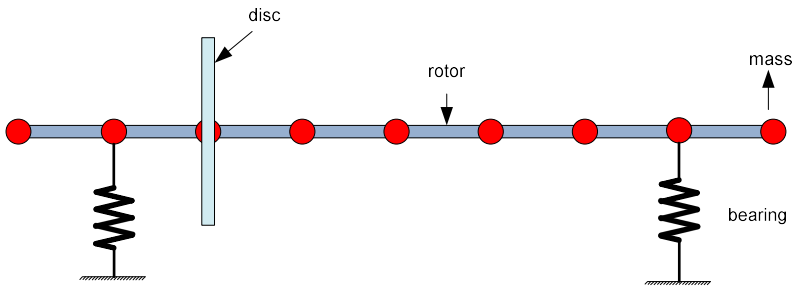

Figure 3.4 Rotor model

The shaft is made of a single material of elastic modulus 2.11×10^{11} Pa and a poison ratio of 0.3. The other parameters are presented in the Table 3.1

Table 3.1 Detailed model parameters of the example rotor-bearing system

S/N	MASS (kg)	IP($kg\cdot m^2$)	ID($kg\cdot m^2$)	L(m)	I($\times10^{-8}m^4$)	E($\times10^{11}$Pa)
1	0.06464801	0	0	0.025	1.64896	2.11
2	0.117669114	0	0	0.044	1.03510	2.11
3	0.106042199	0	0	0.044	1.03510	2.11
4	0.106042199	0	0	0.044	1.03510	2.11
5	0.106042199	0	0	0.044	1.03510	2.11
6	0.109657274	0	0	0.047	1.03510	2.11
7	0.778567374	1.32×10^{-3}	6.76×10^{-2}	0.030	1.03510	2.11
8	0.136478961	0	0	0.032	3.09761	2.11
9	0.100328211	0	0	0	0	0

where, IP- Polar moment of inertia, ID- Diametrial moment of inertia, I- Area moment of inertia, E- Elastic Modulus.

b) ANALYSIS: The system was analyzed for whirl frequencies and mode shape using the Complex Eigenvalue SOLution-107 with direct formulation. Complex LANCZOS method was invoked in solving the abstracted matrix leading to the eigenvalues. The solution was run at 0, 100, 300, and 500 Hz asynchronously, and the real and imaginary roots were determined.

c) RESULTS

WHIRL MODES AND FREQUENCIES: The first four whirl mode of the rotor system is shown in Table 3.2.

Table 3.2 Whirl frequencies and mode

Frequency (Hz)	Backward				Forward			
	Mode 1	Mode 2	Mode 3	Mode 4	Mode 1	Mode 2	Mode 3	Mode 4
0	401.11	655.59	1198.5	2112.4	401.11	655.59	1198.5	2112.4
100	397.38	683.47	1184.2	2107.4	404.51	672.84	1213.8	2117.4
300	388.07	605.61	1159.1	2098	410.21	706.86	1247.9	2128.0
500	376.54	576.01	1138.0	2089.2	414.72	738.89	1286.0	2139.1
700	362.53	550.88	1120.4	2081.0	418.35	767.83	1327.2	2150.7
900	346.32	530.66	1105.6	2073.4	421.31	793.15	1370.1	2162.6

CRITICAL SPEED: The analysis was run at synchronous frequency of 0 to 500 Hz.The result of this analysis is the critical frequency of the system. The result of the analysis is shown in Table 3.3.

Table 3.3 Critical speed

Frequency (Hz)	Forward				Backward			
	Mode 1	Mode2	Mode 3	Mode 4	Mode 1	Mode 2	Mode 3	Mode 4
0-500	383.55	576.01	1093.6	2039.1	412.88	778.16	1494.1	2243.9

d) VERIFICATION OF RESULT: The theoretical Critical frequency obtained by using Campbell diagram (Figure 3.4 below) showed strong correlation with that computed using MD Nastran, thus validation the accuracy of the analysis.

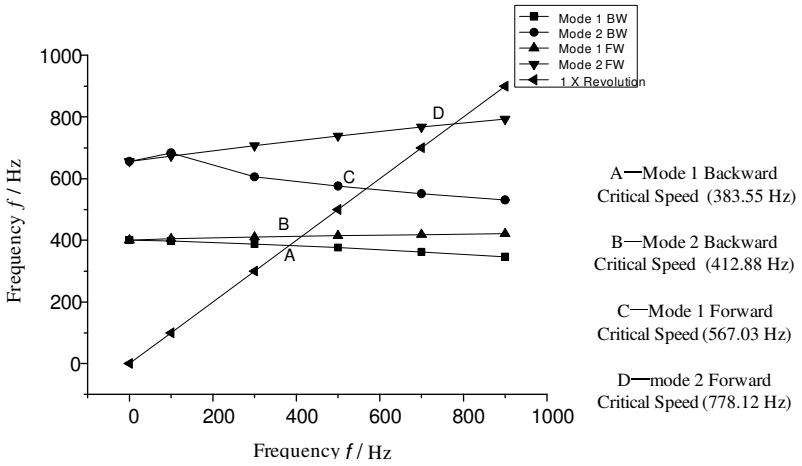

Figure 3.5 Campbell diagram

The result of the analysis from Nastran compared with theoretical Campbell result is presented in Table 3.4.

Table 3.4 Comparison of theoretical and MD-Nastran model critical speed analysis result

Mode	Direction	Theory	MD-Nastran
1	Backward	383.55	383.55
	Forward	412.88	412.88
2	Backward	567.05	567.03
	Forward	778.16	778.12

f) RESULTS: The analysis of Rotor-bearing system had been carried out succefully using MD Nastran solver. The modeling of the system was accomplished using interface tools in Patran program. The system was analyzed for Critical speed and Whirl modes and Frequencies. The result of the Critical speed computed by Nastran showed strong correlation with theorical values computed using Campbell diagram.

3.2 FE Modeling and Analysis of CB-Rotor System in Nastran

3.2.1 CB Model and Analysis

The annotate diagram of the CB structure is shown in Figure 3.6 and contains the housing, MRR, AMB and AMB seat.

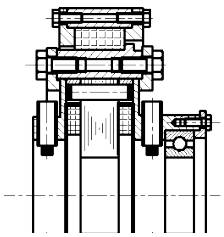

Figure 3.6 Schematic illustration of CB structure

We first developed a 3D finite-element model of MR in free-free condition using HEX element and having 8 nodes. Adopting properties model of equivalent viscous damping and linear stiffness [33], the MR is modeled as circularly distributed BUSH element with lumped mass at each of the nodes. The forces are axially oriented so that tortion can be neglected without much ado. Also, bolts and holes are neglected in the model but the mass contribution is well noted. The total mass of the whole bearing structure is 3.5kg. Other parameters of the MR are; mass 0.857kg, relative density of 1.8×10^3 kg/m^3, poisson ratio 0.02 structural damping 0.1.

The modulus of elasticity and the density shown in Table 3.1 are based on the material properties. Figure 3.7 shows the FE model of metal rubber (a and b) and the housing structure.

Table 3.5 Material properties used in analyses of annulus structure

Name	Material	Elastic Modulus (MPa)	Poisson ratio	Density (kg/m^3)
Housing structure	Aluminum alloy	8.0×10^4	0.3	2.7×10^3
AMB base&Thin metal flap	Carbon steel	2.1×10^4	0.3	7.8×10^3

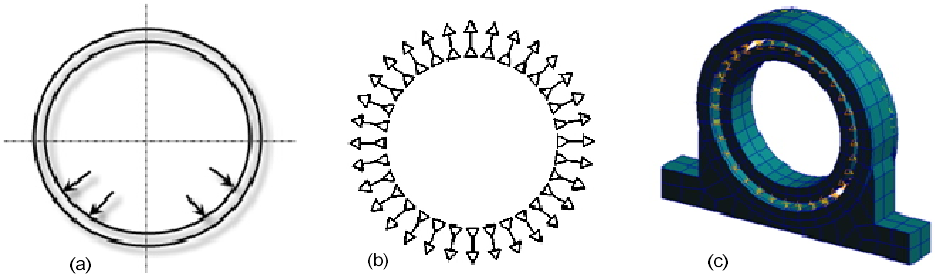

Figure 3.7 Metal Rubber model

Using the method described by [21], the MR is modeled as BUSH element with viscous damping and linear stiffness. The parameters of the MR were obtained using sensitivity-based updating method and obtained as stiffness $4.86\times10^{6}\,\mathrm{N/m}$ by running Complex Eigenvalue analysis using the FE model. The first three mode shapes are shown in Figure3.8. These are the bending vibration (a) and two translation modes (b) and (c) along the vertical and horizontal directions respectively.

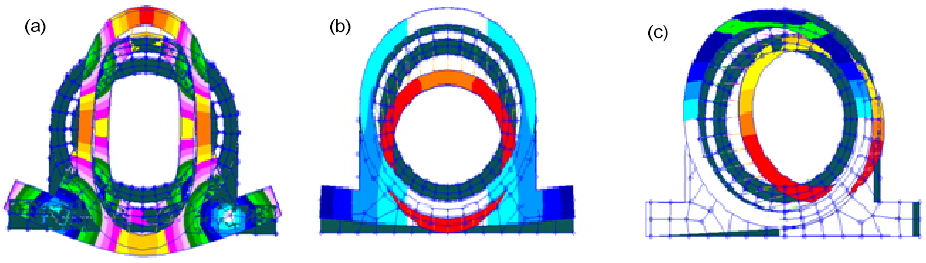

Figure 3.8 Mode shape of the CB by FEA

Table 3.6 compares the result of Complex Eigenvalue analysis of the CB structure from FEM and EMA.

Table 3.6 Comparison of frequency and damping result of EMA and FEM

Mode	EMA		FEM	
	Frequency (Hz)	Damping ratio (%)	Frequency (Hz)	Damping ratio(%)
1	1537.60	0.93	1567.20	0.69
2	2871.69	3.67	2957.18	5.33

3	2896.75	4.65	3027.05	5.62

3.2.2 CB-Rotor Model

Figure 3.9 shows the material used in manufacturing various parts of the rotor. Figure 3.10 shows the FEM model of the rotor.

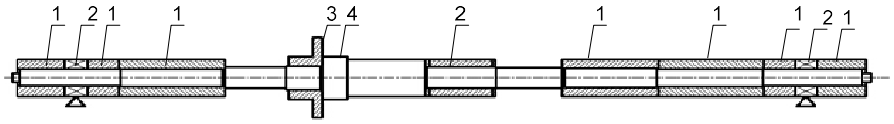

Figure 3.9 Rotor and material make-up

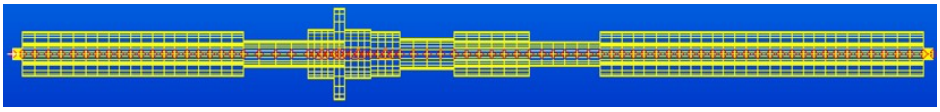

Figure 3.10 Rotor FE model

The rotor comprises of 828mm long iron shaft with copper and iron cover sleeves at some selected cross-sections as shown in Figure 3.9. The material properties of the composite shaft are listed in Table 3.7.

Table 3.7 Material properties of the rotor

	Material	Density (kg / m^3)	E.M (GPa)	Poisson ratio
1	Copper	8430	100.00	0.324
2	Silicon steel	7650	200.00	0.270
3	Pure iron	7860	214.70	0.293
4	Alloy steel	7920	184.00	0.240

In Table 3.7, E.M. means Elastic Modulus.

A built-in electric motor sits at a location half way between the two bearings, and supplies the

rotational torque. The total weight of the composite rotor is 7.35kg. The shaft is discretized into108 Timoshenko beam element between 109 nodes. The sleeves are modeled as shell elements, rigidly connected together and to the rotor at points of interception using BUSH element. Both radial AMB supports are assumed to be symmetrical and isotropic (i.e. $K_{XX} = K_{YY}$). Assuming a linear model for both radial and axial AMB, bush element with stiffness and damping values can be used to model them. We designate AMB and MR physical parameters of stiffness and damping as k_a, c_a and k_m, c_m. Then, k_a and c_a are 4.9×10^5N/m , 3.61×10^2Ns / m respectively as approximated by the PID controller. From experience, we fixed k_m and c_m values at 6.11×10^5N / m and 1.46×10^2Ns / m respectively.

3.3 Analysis Result

3.3.1 Rotor Free-Free

The bearing stiffness and damping are set to low values in order to simulate a free-free condition. At this state, there is no force on the rotor due to the bearing. Complex Eigenvalue analysis solution sequence 107 is exercised using direct method and the eigenvalues and eigenvectors extracted using complex LANCZOS method at a rotation speed of 400 Hz (2513.27 rad/s). The Free-Free analysis is necessary for the placement of the sensors

The first and second bending frequencies were found at 102.25 Hz and 263.17 Hz respectively.

3.3.2 CB-Rotor System

With the rotor in static suspension under the actions of both CB, Complex Eigenvalue analysis Sol 107 was exercised to determine the natural frequencies and damping of the CB-rotor system. The results of the analysis were compared with the EMA test result as shown in Table 3.8.

Table 3.8 Natural frequency and damping ratio comparison of FEA and EMA

Test	Response	1st Bending	2nd Bending
FEA	Frequency (Hz)	54.71	222.77
	Damping ratio (%)	13.13	10.70
EMA	Frequency (Hz)	57.31	225.79
	Damping ratio (%)	16.11	11.05

There is good correlation between the analysis and the test results. With a high confidence level, we compare the dynamic characteristics of CB and AMB systems as presented in Table 3.9.

Table 3.9 CB versus AMB for Natural frequency and damping

Bearing Condition	Response	1st Bending	2nd Bending
CB	Frequency (Hz)	54.714	222.77
	Damping ratio (%)	13.130	10.70
AMB	Frequency (Hz)	58.300	219.80
	Damping ratio (%)	12.200	09.35

Again we see that system on CB has better damping at both bending modes frequencies than does system on only AMB.

3.3.3 Unbalance Response Analysis

Here, an unbalanced static load of 1.0×10^{-6}kg was placed on bearing nodes 9 and 100. The system is rotated at high speed so that the unbalance masses excite flexible mode vibrations. The unbalanced plot is shown in Figure 3.11.

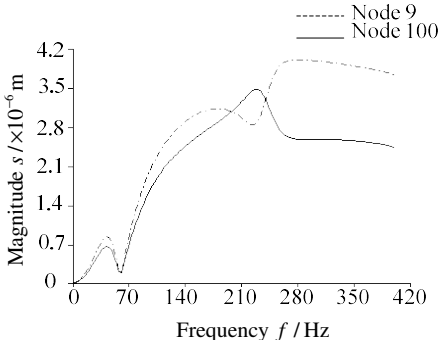

Figure 3.11 Unbalance response of the CB-rotor system

3.3.4 Case Study

OBJECTIVE: to determine the likely range/direction for effective optimal search.

An unbalance of 1.0×10^{-6}kg is placed at the bearing nodes 9 and 100. The system was rotated from 0 to 500Hz. Vibration amplitude at node 9 due to unbalance excitation is measured at same

frequency. The stiffness and damping parameters of the AMB, from experience were set at 355190 N/m and 1801.3Ns/m respectively. Initial MRR stiffness and damping were assumed to be 1.0×10^{6} N/m and 1.0×10^{3} Ns/m respectively.

In this work, we wish to find the ranges of stiffness and damping at which the area under the curve is minimal, and exploit the information in setting the limits of optimal performance.This will be approached in two main steps and four sub-steps.

Case 1: Constant AMB parameter (Stiffness: 355190 N/m, Damping: 1801.3Ns/m).

(1a) High MRR stiffness; (1b) Low MRR stiffness; (1c) High MRR damping; (1d) Low MRR damping.

Case 2: Constant MRR Parameter (Stiffness: 1.0×10^{6} N/m , Damping: 1.0×10^{3} Ns/m).

(2a) High AMB stiffness; (2b) Low AMB stiffness; (2c) High AMB damping; (2d) Low AMB damping

Note: High /low is with respect to initial bearing parameters.

Figure 3.12 shows the effect of varied MRR stiffness on the dynamic response at constant MRR damping and AMB parameters. In the range of second bending critical speed, high MRR stiffness (dotted lines) gave a better dynamic response.

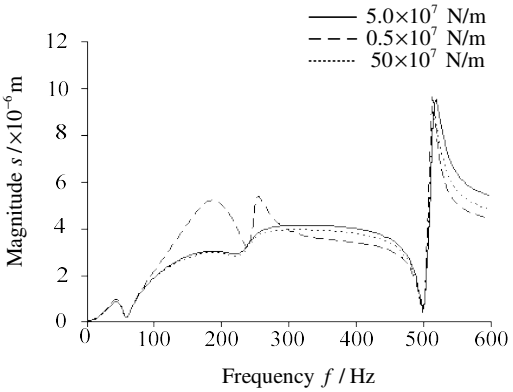

Figure 3.12 Effect of high and low MRR stiffness on dynamics response

However, under flexible mode condition, Low MRR stiffness gives a good dynamics response (long dash line).

Figure 3.13 shows the variation of MRR damping at constant MRR stiffness value.

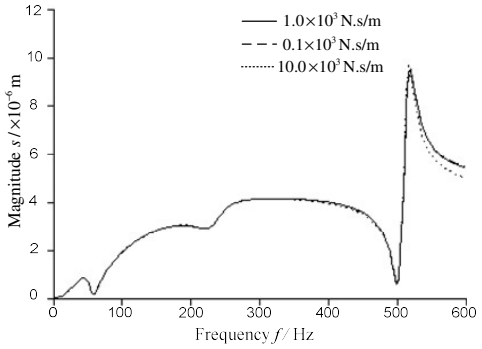

Figure 3.13 Effect of high and low MRR damping on dynamic responds

Within the range of 2nd bending critical speed, increased damping of MRR has better dynamic response.

Figure 3.14 shows the effect of varied AMB stiffness on the dynamic response of the system.

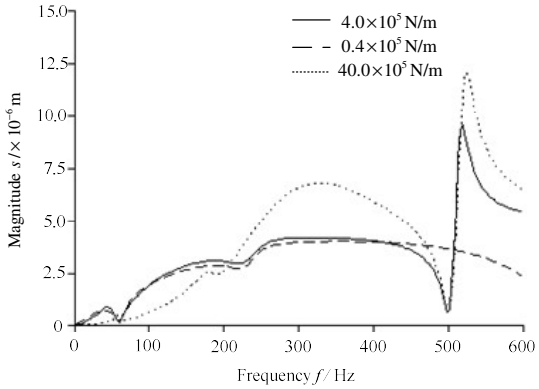

Figure 3.14 Effect of high and low AMB stiffness on dynamic responds

It is seen here that within the range of first bending critical speed, high AMB stiffness has a good effect on the system. However at high frequency, low AMB stiffness has good effect.

Finally, the damping characteristics of AMB are compared in Figure 3.15.

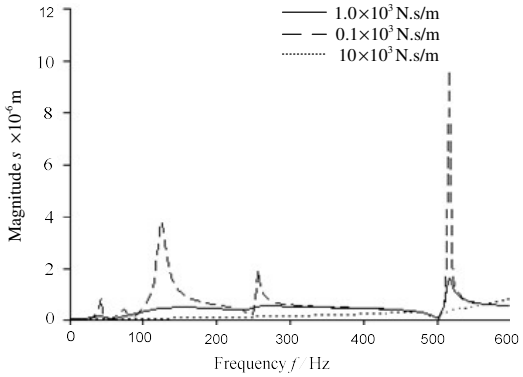

Figure 3.15 Constant MRR parameters at high and low AMB damping

3.4 Chapter Summary

The mathematic model of free-free rotor and Complex Bearing are established respectively and corresponding natrual frequencies are calculated by Nastran. On this basis, the mathematic model of CB-rotor system is established and natural frequencies, modal damping, unbalance response and influence of CB performance parameters on dynamic characteristics of the system are investigated. The main results are:

(1) High MRR stiffness is helpful to restrain the vibration of the rotor operating at the first bending critical speed, while causes much higher vibration of the rotor operating at the second bending critical speed.

(2) Suitable MRR damping is helpful in restraining the vibration of the rotor operating at the first bending critical speed, while has less influence on the vibration of the rotor operating at the second bending critical speed.

(3) The vibration of the rotor decreases with increasing AMB stiffness when the rotor is running at the first and second bending critical speed.

(4) The vibration of the rotor decreases with increasing AMB damping when the rotor is running at the first and second bending critical speed.

Chapter 4 Sensitivity Based Parameter Optimization of CB-Rotor System

4.1 Introduction

Optimization refers to the search for a structural design that is, in some sense, optimal, or "the best," while varying the structure's parameters.

4.1.1 Definition

Analysis model: this is the mathematical idealization of the physical system in order to obtain estimates of certain response quantities. The goal here is to obtain accurate prediction of the responses which can be expected from the real structure.

Design Model: this is an idealized statement of changes which might be made to the structure to improve its performance.

Design Objective: this is function stating the desired response(s) the designer wishes the new or modified design to have.

Design Constraints: these are certain bounds on responses which should not be exceeded while varying the design.

Design Variables are set of parameters of the model used to express what is meant by a suitable variation. Limits on the range of design variables are called "side constraint".

Design Space is the mathematical region over which the design variable, objective and side constraints are not violated or exceeded.

Optimum: This is a sensation used to describe how a product compared in a predetermined desired scale.

Optimization Problem: This refers to series of mathematical equations relating the design objective as a function of design variables. This could be a single- or multi- purpose problem or/ and linear or non-linear function of the design variables.

The general overview of optimization is depicted in Figure 4.1. Structural analysis of the initial design is performed to determine parameters which will drive the optimization. Non-sensitive parameters are screened out. With these parameters that will likely drive the design, the approximate model is formulated. Further analysis is done using this approximate design

model until a pre-determined convergency criterion is met.

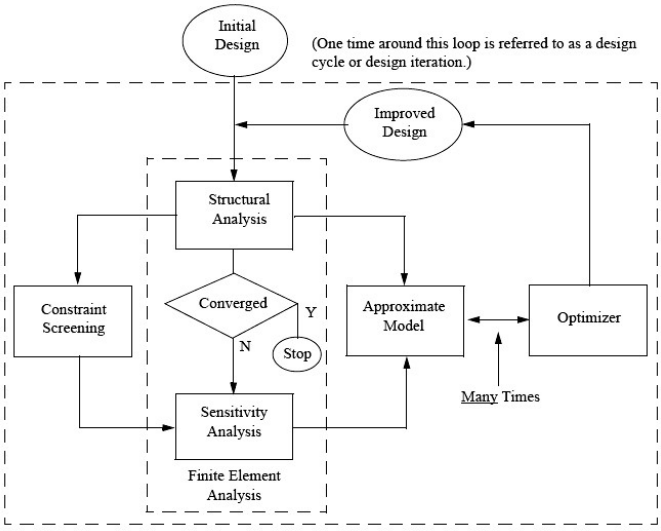

Figure 4.1 MD Nastran implementation of structural optimization

4.1.2 The numerical search process

The numerical search process can be summarized as follows; for a given point in the design space, we determine the gradients of the objective function and the constraints and use this information to determine a search direction. We then proceed in this direction for as far as we can go, whereupon we investigate to see if we are at an optimum point. If we are not, we repeat the process until we can make no further improvement in our objective without violating any of the constraints.

The algorithm can be written as follows;

1) Estimate the start of the design X^0 and set the iteration counter *k*=0. Select a convergence parameter, say $\varepsilon < 0$.
2) Calculate the gradient of $F(X)$ at X^k as $c^k = \forall F(X^k)$.
3) Calculate the vector norm $\|c^k\|$, if $\|c^k\| < \varepsilon$ then stop, otherwise continue.
4) Let search direction at the current point X^k be $d^k = -c^k$.
5) Calculate a step size that minimizes $F(X^k + \alpha d^k)$.
6) Then update the design as $X^{k+1} = X^k + \alpha d^k$ and then $k = k + 1$.
7) Go to step 2 or iteration 2.

4.2 Sensitivity based optimization procedure

Finite element sensitivity based optimization is a valid tool to modify a dynamic model. The sensitivity of such structure's characteristics such as critical speed, damping ratio etc is usually computed and used by the algorithm that searches for the optimum objective function. Modal Assurance Criterion is usually used to compare mode shapes and pairing between two models.

If the design parameter of initial FEM is p, then First Order Taylor Expansion about the function f on p_0 can be written as,

$$f_p(p) = f_p(p_0) + S\Delta p \tag{4.5}$$

where, the residual of function

$$\Delta f(p) = \left\{ f_p(p) - f_p(p_0) \right\} \tag{4.6}$$

and Δp indicates parameter variation, S is sensitivity matrix and is given by, $S = \frac{\partial f_p}{\partial p}|_{p=p_0}$.

So sensitivity based optimization could be considered as the following optimization problem:

$$\min \left\| \varepsilon(p) \right\|_2^2, \varepsilon(p) = \left\{ \Delta f(p) \right\} \tag{4.7}$$

$$s.t. \quad VLB \le p \le VUB \tag{4.8}$$

where p denote design parameter vector, VLB and VUB denote the lower and upper boundary conditions , respectively, $\varepsilon = S\Delta p$ and $\Delta p = S^+ \varepsilon$. Δp indicates parameter variation; S^+ is the generalized inverse about sensitivity matrix S.

Optimization using structural parameters based on sensitivity analysis is an iterative process. Its main steps can be shown as: 1) Select proper parameters p_0 for initial finite element model; 2) Provide the residual error ε form vibration testing and initial finite element model; 3) Calculate the eigenvalue sensitivity matrix with respect to p_0; 4) Compute the parameter variation Δp; 5) Return step 1 to calculate new parameters and to execute all steps until meeting the convergence criterion. It is very important for sensitivity analysis and estimation of correct residual error in optimization.

4.3 Illustrative Example

MODEL DESCRIPTION

The model is a cantilever beam with a circular cross-section shown in Figure 4.2. The goal of this analysis is to match the analytically computed mode shapes to the test mode shapes.

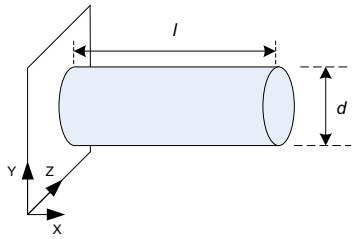

Figure 4.2 Description of the canti lever beam model

The beam has a length of 0.254 m, a diameter of 0.1016 m, poisson ratio of 0.3 and Elastic modulus of 68.95 GPa.

OPTIMIZATION STATEMENT

Objective Function: Minimize the RMS error between the first analytical mode shape (bending mode) and the first test bending mode.

Constraint: The RMS error between the third analytical mode shape (axial vibration mode) and the corresponding third test mode (lateral translation) must be less than 0.002.

Table 4.1 Lateral displacement (T3) and axial displacement (T1)

Grid number	Mode 1		Mode 3	
	Coordinate	Value	Coordinate	Value
3	T3	0.0406	T1	0.2167
6	T3	0.2602	T1	0.6278
9	T3	0.6834	T1	0.9370
Frequency (Hz)	61.912		578.28	

The design variable is the radius of the 3 elements closest to the root of the beam.

MODELING

The canti-lever beam is modeled using 9 c-bar elements constrained in all the 6 DOF at grid 1 and in 2 and 6 (TY and RZ) in the rest of the grid points. The material properties are shown in the diagram.

Given tridiagonalization method was used in the Real Eigenvalue analysis to extract the eigenvalues normalized to unit value of the largest component in the analysis set.

The radius of the three elements closest to the fixed end is used as the design variable. The other seven elements near the free end have the same invariant radius.

The transverse displacements in z-direction for mode 1 (bending mode) and the longitudinal displacement for the mode 3 (extension mode) are chosen as test data.

OPTIMIZATION

For simplicity we present the results as follow

$$X_{\mathrm{A}} = a_{ij} = \begin{bmatrix} a_{11} & \mathrm{L} & a_{1\mathrm{m}} \\ \mathrm{M} & \mathrm{O} & \mathrm{M} \\ a_{\mathrm{g}1} & \mathrm{L} & a_{\mathrm{gm}} \end{bmatrix} \tag{4.9}$$

$$X_{\mathrm{E}} = e_{ij} = \begin{bmatrix} e_{11} & \mathrm{L} & e_{1\mathrm{m}} \\ \mathrm{M} & \mathrm{O} & \mathrm{M} \\ e_{\mathrm{g}1} & \mathrm{L} & e_{\mathrm{gm}} \end{bmatrix} \tag{4.10}$$

$$X_{\mathrm{E}} = \mathrm{E}_{ij} = \begin{bmatrix} \mathrm{E}_{11} & \mathrm{L} & \mathrm{E}_{1\mathrm{m}} \\ \mathrm{M} & \mathrm{O} & \mathrm{M} \\ \mathrm{E}_{\mathrm{g}1} & \mathrm{L} & \mathrm{E}_{\mathrm{gm}} \end{bmatrix} \tag{4.11}$$

where X_{A}, X_{E} and X_{E} are the analytical, experimental and error matrices, ε_{ij} a_{ij}, e_{ij} and are elements , subscript i, j (i=1 to g, j=1 to m) are the grid positions and mode respectively.

$$X_{\mathrm{E}} = X_{\mathrm{A}} - X_{\mathrm{E}} = \{\mathrm{E}_{ij}\} \tag{4.12}$$

$$\mathrm{E}_{ij} = e_{ij} - a_{ij} \tag{4.13}$$

In this work, we are interested in j = 1, 3 .i.e.T3 displacement for bending mode 1 and T1 displacement for longitudinal mode 3) at grid points i=3, 6 and 9.

So we have,

$$X_{\mathrm{A}} = \begin{bmatrix} a_{31} & a_{33} \\ a_{61} & a_{63} \\ a_{91} & a_{93} \end{bmatrix} \tag{4.14}$$

$$X_{\mathrm{E}} = \begin{bmatrix} e_{31} & e_{33} \\ e_{61} & e_{63} \\ e_{91} & e_{93} \end{bmatrix} \tag{4.15}$$

$$X_{\mathrm{E}} = \begin{bmatrix} \mathrm{E}_{31} & \mathrm{E}_{33} \\ \mathrm{E}_{61} & \mathrm{E}_{63} \\ \mathrm{E}_{91} & \mathrm{E}_{93} \end{bmatrix} \tag{4.16}$$

$$X_{\mathrm{E}} = (\mathrm{E}_1, \mathrm{E}_3) \tag{4.17}$$

$$E_1 = \begin{Bmatrix} E_{31} \\ E_{61} \\ E_{91} \end{Bmatrix} E_3 = \begin{Bmatrix} E_{33} \\ E_{63} \\ E_{93} \end{Bmatrix} \tag{4.18}$$

evaluated from (4.16), the Euclidean norm of the error $i = 1,\ 3$ is to be minimized.

Mathematically the optimization problem can be presented as follows

$$\text{Min} \left\| E_1(R) \right\|_2^2, \tag{4.19}$$

Subject to,

$$\left\| E_3(R) \right\|_2^2 \le 0.002 \tag{4.20}$$

RESULTS/DISCUSSION

The job was executed in MSC.Nastran SOL 200.

In Nastran, design objective is defined in CASE CONTROL section by the DESOBJ. Design variable is defined in the BULK DATA section by DESVAR and design constraint is defined in the BULK DATA section by DCONSTR.

As a start, the optimizer performs analysis to determine the current state of the responses. The result of such initial analysis is shown below.

INTERNAL ID	DRESP1 ID	RESPONSE LABEL	GRID ID	COMPONENT NO.	MODE	LOWER BOUND	VALUE	UPPER BOUND
1	511	MDISP13	3	3	1	N/A	6.6205E-02	N/A
2	512	MDISP16	6	3	1	N/A	3.4278E-01	N/A
3	513	MDISP19	9	3	1	N/A	7.2745E-01	N/A

----- EIGENVECTOR DISPLACEMENT RESPONSES -----

INTERNAL ID	DRESP1 ID	RESPONSE LABEL	GRID ID	COMPONENT NO.	MODE	LOWER BOUND	VALUE	UPPER BOUND
4	514	MDISP33	3	1	3	N/A	3.0902E-01	N/A
5	515	MDISP36	6	1	3	N/A	7.0711E-01	N/A
6	516	MDISP39	9	1	3	N/A	9.5106E-01	N/A

---- RETAINED DRESP2 RESPONSES ----

INTERNAL ID	DRESP2 ID	RESPONSE LABEL	EQUATION ID	LOWER BOUND	VALUE	UPPER BOUND
1	500	DIFM1	550	N/A	9.7038E-02	N/A
2	700	DIFM3	750	N/A	1.2251E-01	2.0000E-03

Figure 4.3 Nastran extract; Modal shape data

From the analysis result displayed by Nastran we can extract the necessary information to show how optimization is performed. T3 and T1 at grids 3, 6 and 9(highlighted in red and blue respectively) are displayed in matrix form below.

$$X_A = \begin{bmatrix} 0.0662 & 0.3090 \\ 0.3428 & 0.7071 \\ 0.7274 & 0.9511 \end{bmatrix} \quad X_E = \begin{bmatrix} 0.0406 & 0.2167 \\ 0.2602 & 0.6278 \\ 0.6834 & 0.9370 \end{bmatrix}, \text{ thus } \quad \mathrm{X_E} = \begin{bmatrix} 0.0256 & 0.0923 \\ 0.0826 & 0.0793 \\ 0.0440 & 0.0141 \end{bmatrix}$$

The above result of $\mathrm{X_E}$ can be split into

$$\mathrm{E_1} = \begin{Bmatrix} 0.0256 \\ 0.0826 \\ 0.0440 \end{Bmatrix}, \text{ and } \mathrm{E_3} = \begin{Bmatrix} 0.0923 \\ 0.0793 \\ 0.0141 \end{Bmatrix}$$

The objective function $\|E_1(R)\|_2^2$ is then computed from the above two error as follows;

$$= \sqrt{0.0256^2 + 0.0826^2 + 0.0440^2} \;\; = \;\; 0.0970$$

$$= \sqrt{0.0923^2 + 0.0793^2 + 0.0141^2} \;\; = 0.1225$$

This is exactly the same with the response computed by Nastran (highlighted in yellow).

As can be seen from the result, the constraint is badly violated. The first task of the optimizer is to return the design to the feasible region using modified method of feasible direction. This method establishes a search direction tangential to the constraint about being violated (critical constraints). Once this had been achieved, it proceeds to minimization of the objective function.

Note: Since we have only one design (decision) variable the sensitivity matrix is 1×8 (ie 6 from grid 3, 6 and 9 responses for mode 1 and 3, and 2 from the DRESP2 that specifies the objective function and constraint).i.e.

$$\nabla F(X) = \frac{\partial y_1}{\partial x}, \frac{\partial y_2}{\partial x}, \frac{\partial y_3}{\partial x}, ..., \frac{\partial y_8}{\partial x} \tag{4.21}$$

The sensitivity computed by Nastran is shown in the Figure 4.4.

OBJECTIVE AND MAXIMUM CONSTRAINT HISTORY

CYCLE NUMBER	OBJECTIVE FROM APPROXIMATE OPTIMIZATION	OBJECTIVE FROM EXACT ANALYSIS	FRACTIONAL ERROR OF APPROXIMATION	MAXIMUM VALUE OF CONSTRAINT
INITIAL		9.703752E-02		6.025679E+01
1	1.340757E-02	3.335541E-02	-5.980392E-01	1.782543E+01
2	2.236070E-04	4.787858E-03	-9.532971E-01	1.526480E+00
3	2.640505E-05	1.483425E-04	-8.219994E-01	N/A
4	4.717481E-05	4.683008E-05	7.361399E-03	N/A
5	4.683008E-05	4.683008E-05	0.000000E+00	N/A

SUBCASE 1001

DESIGN VARIABLE HISTORY

INTERNAL DV. ID.	EXTERNAL DV. ID.	LABEL	INITIAL	1	2	3	4	5
1	101	RAD1	2.0000E+00	1.6450E+00	1.5191E+00	1.4995E+00	1.4989E+00	1.4989E+00

* USER INFORMATION MESSAGE 6464 (DOM12E)

Figure 4.4 Nastran extract; sensitivity result against design cycle

Figure 4.5 shows the variation of the design variable i.e. the radius with the optimization cycle (a) and (b) decrease of the Euclidean norm (error) with design cycle.

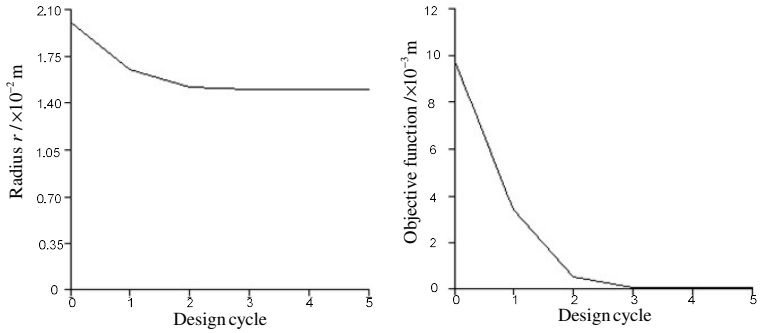

Figure 4.5 (a) Variation of design variable (a) and objective function (b) with design cycle

4.4 Case Study

The description and modeling of the rotor have been treated in section 3.2.2. The responses for optimization are the natural frequencies and damping ratio. It is desired the damping be increased so that the system can operate beyond bending critical speed occurring at 250 Hz. The responses of interest will be based on complex modal analysis.

Neglecting the excitation force, single value decomposition of (3.18) results to the right, u_i and left, v_i eigenvectors of *i-th* eigenvalue λ_i given below;

$$(\lambda_i^2 M^T + \lambda_i (C_d + G)^T + K^T)\{u_i\} = 0 \tag{4.21}$$

$$(\lambda_i^2 M^T + \lambda_i (C_d + G)^T + K^T)\{v_i\} = 0 \tag{4.22}$$

$$\lambda_i = \alpha_i \pm \omega_i \tag{4.23}$$

where *D* matrice in (3.18), has been replaced by damping matrice C_d and gyroscopic matrice *G*.

The idea behind the optimization is that the modal parameters (damping coefficient, α_i and frequency ω_i) of a mode, i can conveniently be adjusted to assume a preassigned value. This is the job

of optimization algorithm.

Maximize:

$$f(p)=\sum_{i=1}^{N} A_i\xi_i + B_i\omega_i \quad (4.24)$$

s.t.

$$\frac{\omega_j}{\varpi_j}-1\le 0 \qquad j=1,...,k \quad (4.25)$$

$$g_{k+1}:\frac{m}{m_{\max}}-1\le 0 \quad (4.26)$$

$$p_i^l \le p_i \le p_i^u \quad i=1,...,n \quad (4.27)$$

where, A_i and B_i are weighting factors associated with each modal damping ξ_i and frequency ω_i respectively, ϖ_i is the desired modal frequencies for each mode. k is the total number of modes of interest, m and $m_{\max}$ are the overall mass and maximum allowable mass of the structure, respectively.

For the rotor structure under study, the natural choices for the design variables p_i in (4.24) are the bearing parameters; the stiffness and damping of the AMB (k_a, c_a), the stiffness and damping of MRR (k_m, c_m) and the mass of the AMB (m_a).

The complex eigenvalue design sensitivity can be derived by differentiating (4.21) and (4.22) with respect to design variable. The approximation for the variation in the *k-th* complex eigenvalue [9] is given by:

$$\Delta\lambda_i=\frac{\partial\lambda}{\partial p_i}=\frac{-\{v_i\}^T\left([\Delta M]\right)\lambda_i^2[\Delta(C_d+G)]\lambda_i+[\Delta K]\{u_i\}}{\{v_i\}^T\left(2\lambda_i[M]+[(C_d+G)]\right)\{u_i\}} \quad (4.28)$$

where, P_i, i = 1, 2, … n, are vector of the design variables.

These analyses are carried out in MSC/MD Nastran Finite Element Software.

Table 4.2 Pre-optimization CB parameter values

Design Variable	Value	Initial	Lower bound	Upper bound
k_a (N/m)	355190.0	1	0.2	10
c_a (Ns/m)	1801.3	1	0.2	10
k_m (N/m)	100000.0	1	0.2	10

c_a (Ns/m)	10000.0	1	0.2	10

Sequential Quadratic Programming (SQP) was used by Nastran optimizer to estimate the value of the objective function between iterations. The modes of interest are the 1st and 2nd bending modes designated as mode 1 and mode 2 respectively. The optimization results are shown in Table 4.3 and Table 4.4 for modes 1 and mode 2 respectively. The pre-optimization modal natural frequency and damping ratio are 95.61Hz and 8.36 % respectively for mode 1. Those for mode 2 are 255.92 Hz and 5.68% respectively. Convergence was achieved in 19th iterative cycles of the re-design process and the optimum was found at 106.65 Hz, 43.18% for mode 1 and 254.24 Hz, 8.40% for mode 2.

Table 4.3 Summary of optimization result for mode 1

Cycle	Damping	Frequency(Hz)	Damping ratio
1	25.1273	95.61876	0.083647
2	28.4658	103.7104	0.087368
3	36.7618	105.7505	0.110653
4	47.8812	106.3667	0.143288
5	56.4744	106.2608	0.169172
6	73.2539	106.8693	0.218186
7	97.6147	106.9608	0.290497
8	105.619	107.4983	0.312743
9	114.760	106.7455	0.342209
10	119.193	107.2534	0.353743
11	122.338	106.9425	0.364135
12	127.703	106.6638	0.381094
13	130.107	106.9846	0.387105
14	131.899	106.6216	0.393773
15	134.899	106.6517	0.402615
16	137.537	106.5908	0.410722
17	138.499	106.8087	0.412753
18	141.762	106.6530	0.423093
19	144.689	106.6507	0.431840

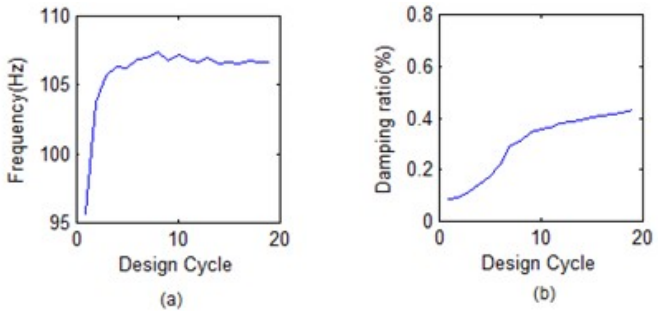

Figure 4.6 Plot of frequency (a) and damping ratio (b) against design cycle for mode

Table 4.4 Summary of optimization result for mode 2

Cycle	Damping	Frequency(Hz)	Damping ratio
1	45.6792	255.92	0.056814
2	65.1264	256.16	0.080928
3	93.0148	254.41	0.116376
4	106.985	247.78	0.137438
5	73.2967	249.67	0.093448
6	74.6930	250.18	0.095034
7	75.2053	250.84	0.095433
8	67.8952	252.75	0.085507
9	71.1291	252.75	0.089581
10	67.3129	253.54	0.084507
11	66.2855	253.75	0.083149
12	67.5772	253.76	0.084767
13	64.6881	253.83	0.081119
14	66.1459	253.82	0.082951
15	66.4044	253.92	0.083243
16	67.0703	253.93	0.084075
17	65.9264	253.97	0.082627
18	67.0163	254.11	0.083947
19	67.0772	254.25	0.083979

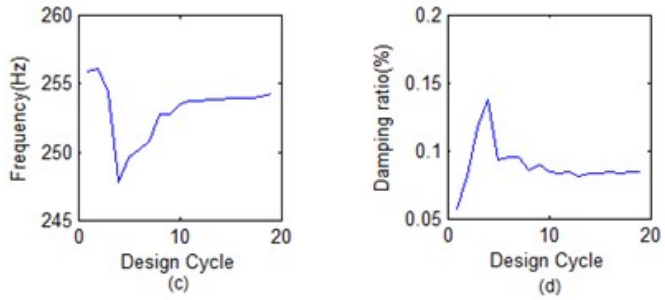

Figure 4.7 Plot of frequency (c) and damping ratio (d) against design cycle for mode 2

The unbalance plot for the system before (dotted) and after (solid) optimization are shown in Figure 4.8.

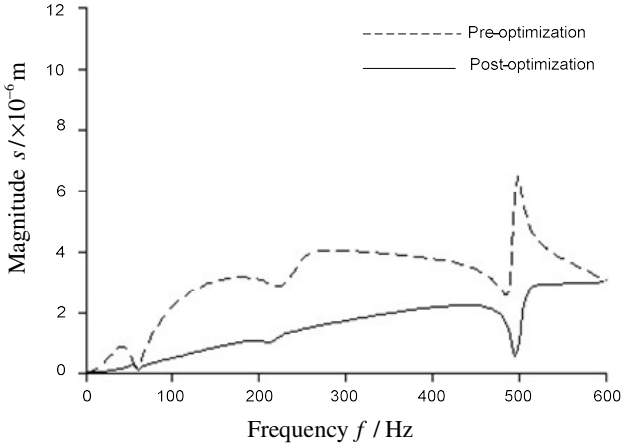

Figure 4.8 Comparison of unbalance response plot of system before and after optimization.

4.5 Chapter Summary

In this chapter, finite element sensitivity based optimization method for the CB-rotor system was illustrated. Aiming at obtaining high damping ratios within the regions of bending critical speeds, a case study with 4 design variables was conducted using Nastran solution 200. Both the example and real case study proved the proposed optimization method as valid. The first bending mode damping ratio changes from 0.08 to 0.43, while the second bending mode damping ratio changes from 0.05 to 0.08.

Chapter 5 Experimental Research of the System

The natural, frequencies, damping ratios and response levels predicted by analytical models are generally not satisfactory unless validated by experimentally obtained data. For this purpose, we usually employ two kinds of tests; Experimental Modal Analysis (EMA) and actual operation of the system.

5.1 Experimental Modal Analysis

In EMA, we seek to extract the vibration modes (i.e. natural frequencies, mode shapes, and damping coefficients) of a structure from its response to excitation input. Through this information we can tell the dynamic behavior of the structure.

5.1.1 Apparatus in EMA

Main apparatus for EMA test are;

1) CA-YA-186 Accelerometer with axial sensitivity of 100mV/g.
2) 5110 Impact hammer. Sensitivity of 3.73mV/N.
3) Agilent 35670A Dynamic Signal Analyzer (DSA).
4) N-Modal Modal Identification Software.

The procedure for EMA is shown in Figure 5.1. Vibration is induced into the test structure using the Impact hammer. The hammer is equipped with load cell which records the magnitude of the force on impact and send the information to the Agilent 35670A Digital Signal Analyzer. With the placement of CA-YA-186 accelerometer at a pre-determined location, the vibration displacements is sensed and relayed to the DSA. Care was taken to ensure that the accelerometer be not placed at the node location. The DSA processes this information by dividing the displacement vector by the force to derive them in necessary results. This is depicted in Figure 5.1.

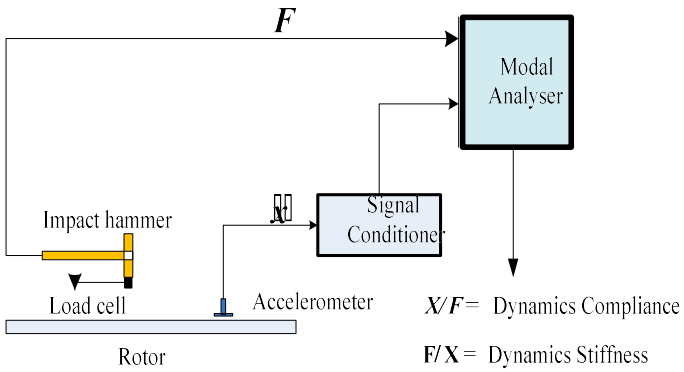

Figure 5.1 Modal analysis schematic diagram

Figure 5.2 shows the experimental Test environment: 1) Mechanical unit. 2) Electronics unit. 3) Recording and measurement unit.

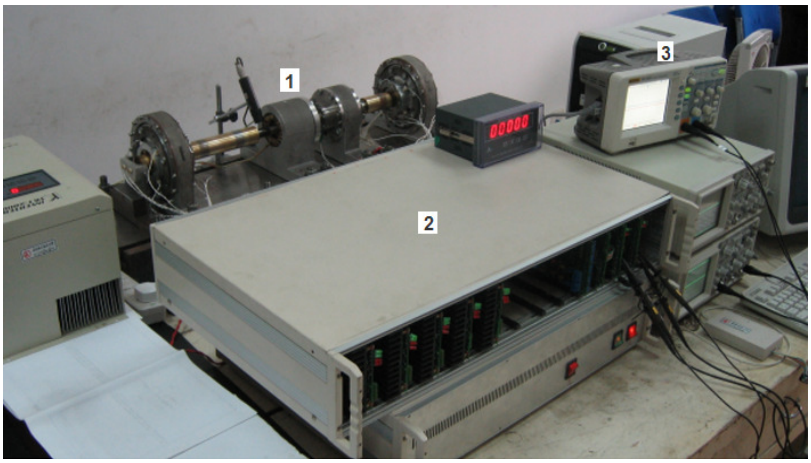

Figure 5.2 Laboratory test environment

5.1.2 EMA for Free-Free Rotor

This test is necessary for the design of bearings and placement of sensors.The apparatus are arranged as shown in the Figure 5.3 and 5.4. The specimen rotor is marked out on 17 choosen locations as shown in Figure 5.4. These are the input (excitation) and output (displacement) locations. It is then rested on an inflated tube to ensure an almost no-stiffness support condition.

Figure 5.3 Rotor-only EMA test set-up

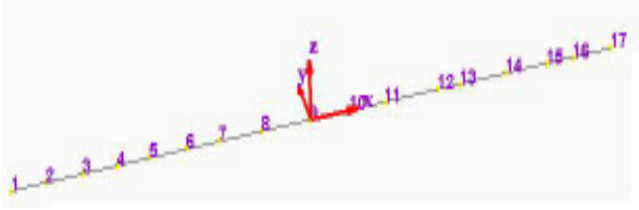

Figure 5.4 17-Excitation position of free-free rotor

Modal frequencies and modal shapes are shown in Table 5.1 and Figure 5.5. Table 5.1 shows that, the results of EMA for free-free rotor are in good agreement with theoretical analysis results.

Table 5.1 Rotor-only modal frequencies and shapes

Mode number	1	2	3	4
Frequency(Hz)	97.81	249.01	493.66	810．02

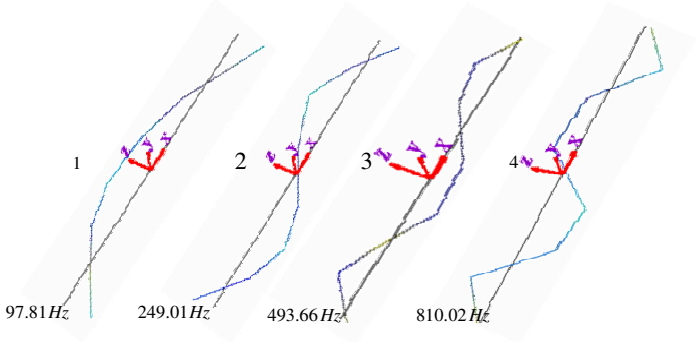

Figure 5.5 Rotor free-free mode shapes and frequencies

5.1.3 EM A for CB-Rotor system

In this test, the rotor is supported on CB so that the influence of the bearing stiffness and damping on the system dynamic can be realized.

The procedure for CB-Rotor EMA is described using the flow diagram as shown in Figure 5.6.

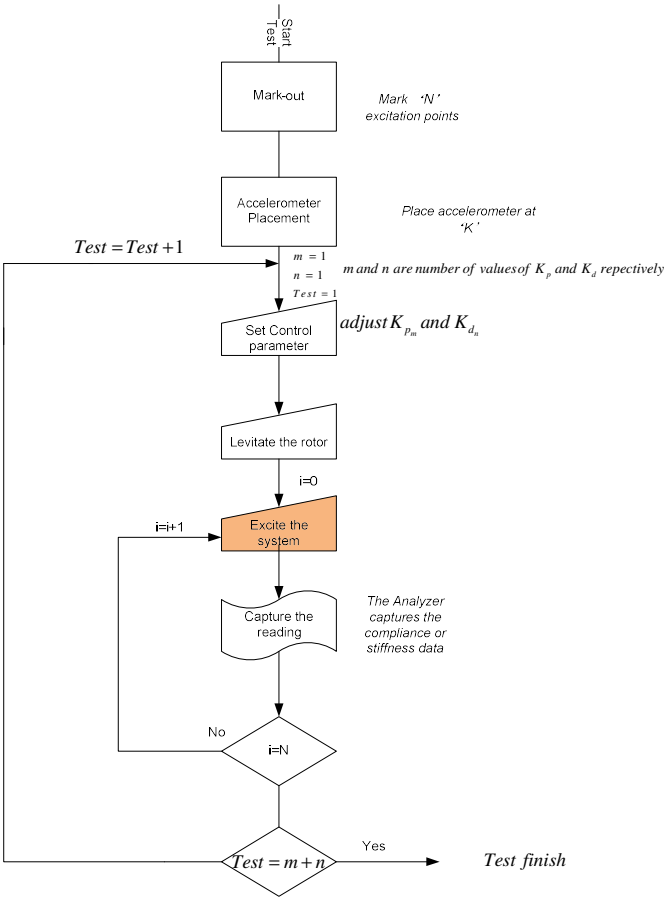

Figure 5.6 Flow chart illustration of the Procedure for EMA test

a) Mark out the input and output locations *N*.

b) Place the accelerometer at a choosen location using plasticin. Care should be taken to avoid the node.

c) Set the stiffness and damping through the controller.

d) Start the system to levitate the rotor.

e) Apply excitation at the first location as marked in a).This should be done as swiftly as

possible to ensure no-time lapse.

f) Capture the reading displayed on DSA.

g) Repeat step e) to f) for the next input locationfor all the marked locations.

h) Repeat step c) to g) for all the possible set of AMB parameter.

i) Stop test.

Locations of the input and out put points are shown as Table 5.2 and Figure 5.7.

Table 5.2 Rotor input/out put points

Number	Axial location（cm）	Location of Accelerometer
1	0	no
2	11.5	no
3	16	no
4	20.5	no
5	34.5	no
6	41.5	yes
7	47	no
8	51.5	no
9	60.5	no
10	64	yes
11	68	no
12	78.5	no

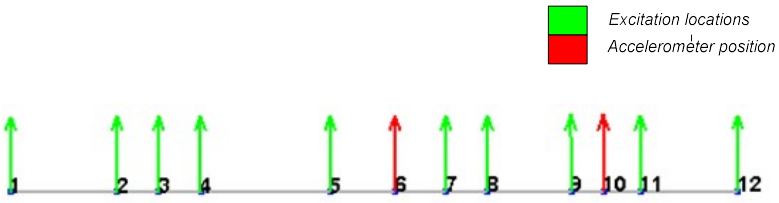

Figure 5.7 Excitation and response position of CB-rotor system

The Analyzer double-integrates the acceleration signal which it uses to, in conjuction with the excitation force information generate either the compliance or the dynamic stiffness data. This data is inputed into N-Modal software to generate relevant plots.

The rotor is stably suspended by the action of the CB. The parameters of the controller are given in Table 5.3 below.

Table 5.3 Control parameters of AMB

K_p	K_i	K_d	$T_d(s)$
2.55	16.61	6.9×10^{-3}	1.12×10^{-5}

By the excitation tests, the curves of the driving point frequency response function in the 6th and 10th positions are shown in Figure 5.8. Also the curves of the cross-point frequency response function between the 6th position and the 10th position are shown in Figure 5.9.

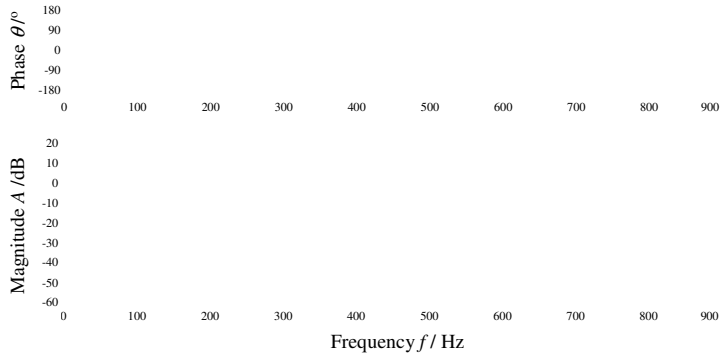

Figure 5.8 Driving point frequency response plot of CB-rotor EMA test

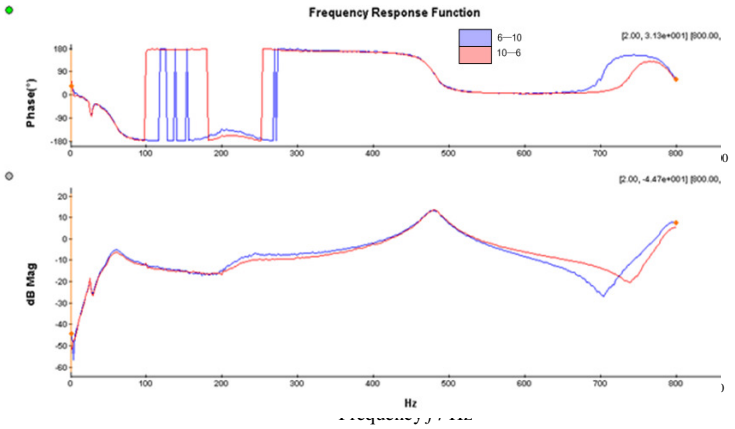

Figure 5.9 Cross-point frequency response plot of CB-rotor EMA test

Similarly, the first five mode shapes can be obtained, as shown in Figure 5.10. The values of the first five mode frequencies and the corresponding modal damping ratios of the system are shown in Table 5.4.

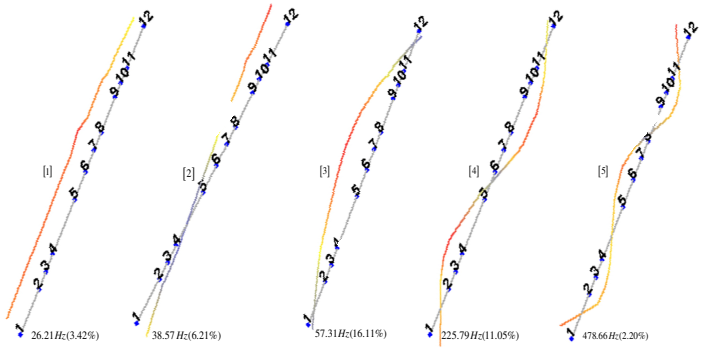

Figure 5.10 Modal frequencies and shapes from CB-rotor EMA test

Table 5.4 First five mode frequencies

Mode number	1	2	3	4	5
Frequency(Hz)	26.21	38.57	57.31	225.79	478.66
Damping ratio (%)	3.42	6.21	16.11	11.05	2.20

The EMA of CB-rotor system shows that, the first four modal damping ratios values are high. This is helpful for the system to get across the first two bending critical speeds safely.

5.2. Actual Operation of the system

In actual operation of the system, the rotor, stably suspended by the action of the CB and driven by high power built-in motor runs from 0 to 16800rpm. The vibration of the rotor due to unbalance rotation is sensed by eddy current displacement sensors. Sensitivity of the sensor is 16666.67V/m. The vibration signal picked by the sensor collocated firmly with the actuator of the right CB is transmitted to the Agilent 35670A DSA for processing.

The control parameters are shown in Table 5.5, and the resultant stiffnesses and Damping are shown in Table 5.6.

Table 5.5 Control parameter of AMB

K_p	K_i	K_d	T_d(s)
2.55	16.61	6.9×10^{-3}	1.12×10^{-5}

Table 5.6 AMB equivalent stiffness and damping

Stiffness(N/m)	Damping(N.s/m)
3.55×10^{5}	1.80×10^{3}

The vibrations of the rotor are plotted against rotational speed as shown in Figure 5.11.

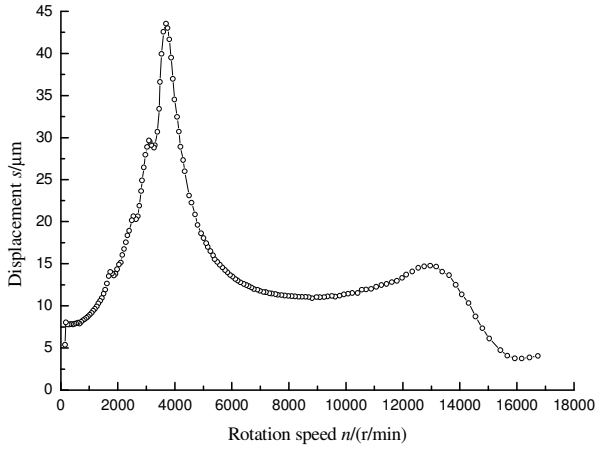

Figure 5.11 System's actual operation unbalance response

Fig.5.11 shows that the CB-rotor system can pass through the first two bending critical speeds safely.

5.3 Chapter Summary

Dynamic characteristics of the system supported by the complex bearings are studied by Experimental Modal Analysis and actual operation of the system. The results show that the first four modal damping ratios of the system are heavy, and the system can get across the first two bending critical speeds safely.

Chapter 6 Conclusion and Future Work

6.1 Main Work and Conclusion

Dynamic characteristics and Parameters Optimization of the system supported on Complex Bearing are studied in this thesis by theoretical analysis, Experimental Modal Analysis and actual operation. The main work and conclusions are as follows;

1) Critical speed analysis of demonstrative bearing-rotor system has been carried out by MD Nastran, and the results showed strong correlation with values obtained by Campbell diagram.
2) The mathematic model of free-free rotor and Complex Bearing are established respectively and corresponding natrual frequencies are calculated by Nastran.
3) The mathematic model of CB-rotor system is also established and used to analyze natural frequency, modal damping, unbalance response. The influences of CB performance parameters on dynamic characteristics of the system are investigated. The results showed that, both MRR and AMB stiffness and damping are sensitive to the unbalance responses of the system and have complicate relationship to dynamic characteristics of the system.
4) Aiming at obtaining high critical speeds and large damping ratios, a case study with five design variables was conducted by using Nastran solution 200. The results show that the proposed optimization method was valid, the first bending mode damping ratio changes from 0.08 to 0.43, while the second bending mode damping ratio changes from 0.05 to 0.08.
5) Dynamic characteristics of the CB-rotor system are investigated by Experimental Modal Analysis and actual operation of the system. The results are in good agreement with theoretical analysis results and show that the first four modal damping ratios of the system are heavy, and the system can get across the first two bending critical speeds safely.

6.2 Future Work

1) The design parameters used in the thesis do not include the positions of the CB bearings. Of course, the position of the bearing plays important role in control. Next levels of modal parameter optimization have to consider inclusion of dimension and the position parameter.
2) In this thesis, only two bearings were used. In fact, a flexible rotor may require more bearings to make the whole system have good dynamic characteristics.

References

[1] Gehrald Schweitzer. Applications and Research Topics for active magnetic bearings. Proc. Symp. on Emerging Trends in Rotor Dynamics, Indian Institute of Technology, Delhi, India. Springer-Verlag, March 23-26, 2009.

[2] Earnshaw S．On the nature of the molecular forces which regulate the constitution of the lumiferons ether．Trans．Camb．Phil，Soc7，1842：97-112．

[3] Kemper H．overhead suspension railway with wheelless vehicles employing magnetic suspension from iron tails．Germ．Pat．Nos．643316 (1937) and 644302 (1937)．

[4] Angantyr Anders. Rotordynamic optimization of Large Turbo System using Genetic Algorithm. [PhD Thesis]. Lulea University of Technology, 2006.

[5] Fitrial, A. S. System Identification and Control of Magnetic Bearing Systems. [PhD Thesis]. USA: Univ. Victoria, 2007.

[6] Hung, J. Y. Nonlinear Control of Electromagnetic Systems. Proc. 17th Annu. Conf. IEEE Ind. Electron Soc., Kobe, Japan, 1991.

[7] Hong, S. K., R. Langari. Fuzzy Modeling Control of a Nonlinear Magnetic Bearing System. Proc. of the IEEE International Conference On Control Applications, 1997.

[8] Chen, S.T., Lee, A.C. Decoupling vibration control of a flexible rotor system with symmetric mass and stiffness properties. Proceedings of Institute of Mechanical Engineers, 1993, 207:9 -14.

[9] Nonami, K., Yamanaka T., M. Tominaga. Vibration and control of a flexible rotor supported by magnetic bearings. JSME International Journal, 1990, Series III 33 (4):475–482.

[10] Lee, A.C., Chen, S.T., Optimal vibration control for a flexible rotor with gyroscopic effects, JSME International Journal, 1992, Series III 35 (3): 446–455.

[11] Salm, J.R. Active electromagnetic suspension of an elastic rotor: modeling, control, and experimental results. Journal of Vibration, Acoustics, Stress, and Reliability in Design, 1988:110: 493–500.

[12] Burrows, C.R., Keogh, P.S. and Tasaltin, R. Closed-loop vibration control of flexible rotors - an experimental study, Proceedings of the Institution of Mechanical Engineers, Part C: Journal of Mechanical Engineering Science, 1993,207 (1):1–17.

[13] Knospe, C.R., Hope, R.W., Fedigan, S.J. Williams, R.D. Experiments in the control of

unbalance response using magnetic bearings, Mechatronics, 1995, 5 (4): 385–400.

[14] Yu Z. Meng L.T. King, L.M. Electromagnetic bearing actuator for active vibration control of a flexible rotor. Proceedings of the Institution of Mechanical Engineers, Part C: Journal of Mechanical Engineering Science1998 212(8): 705–716.

[15] Shida H. Motion and Vibration Control of Flexible Rotor Using Magnetic Bearings. Proc. Of the 8th International Symposium on Magnetic Bearings, CD-ROM, 2002.

[16] Soe Jeon.Model Validation and controller Design for Vibration Suppression of Flexible Rotor Using AMB.KSME Int. Journal, 2002, 16 (12): 1583-1593.

[17] Fujiwara H. Control of Flexible Rotors Supported by Active Magnetic Bearings. Proc. of the 8th International Symposium on Magnetic Bearings, CD-ROM, 2002.

[18] Hamburg G, Parkinson J. Gas Turbine shaft dynamics, SAE Trans., 1962, 70: 774-784

[19] Jastrzebski R. P. and Pollanen R. Observer-based Unbalance Compasation in LQ Control of AMBs. Proc. of the 11th International Symposium on Magnetic Bearings, 2008.

[20] Friedericy J. A., Eppink R. T., Liu Y. N., Cetiner A. An Investigation of the Behavior of Floating Ring Dampers and the Dynamics of Hypercritical Shafts on Flexible Supports.USAAML Technical Report 65-34, UVA Report No. E-3340104-65, 1965.

[21] Nicholas J.C., Barrett L.E.The Effect of Bearing Support Flexibility on Critical Speed Prediction. ASLE Transactions, 1986: 29(3).

[22] Barrett L.E., Nicholas J.C., Dhar D. The Dynamic Analysis of Rotor-Bearing Systems Using Experimental Bearing Support Compliance Data. Proceedings of the 4th International Modal Analysis Conference, Union College, Schenectady, New York, 1986: 2, 1531-1535.

[23] Wang S.C., Deng Z.Q., Gao H.B. Experimental Investigation of Mechanical Property of the Metal Rubber Used in Lunar Lander in High or Low Temperature. J.Aeronaut Mater, 2004, 24: p.271.

[24] Gao Hua. Dynamic Characteristics of Magnetic Bearing System with Metal Rubber Annuluses, [Master's Thesis], Nanjing, Nanjing University of Aeronautics and Astronautics, 2009.

[25] Xie Zhen-yu, Wang Tong, Zhang Jing-ting. Dynamic characteristics of active magnetic bearing system with metal rubber annuluses. Journal of Aerospace Power, 2009, 24(2): 378-383.

[26] FEA Learning Center, Academics. An Interactive tutorial. MSC Software Corporation, Santa Ana, CA, USA, 2010.

[27] Bucher I, Ewins D.J. Modal analysis and testing of rotating structures. Phil. Trans. R.Soc. Lond, 2001, 359: 61~96.

[28] Schweitzer G., Maslen E.H. Magnetic Bearings. New York: Springer, 2009:31.

[29] Swanson Erik E. L., Maslen E.H., Cloud C. H. Rotor dynamic Design Audit of AMB supported machinery. Proceeding of the thirthy-seventh Turbomachiery symposium, 2008.

[30] Genta G. Vibration of Structure and Machines. New York: Springer-Verlag, 1999.

[31] Meirovitch L. Fundamental of Vibration, New York, McGraw-Hill, 2000.

[32] Cook R. D., Malkus D. S. Plesha, M. E. Concept and Application of Finite Element Analysis. New York, John Wiley and Sons, 1989.

[33] Qing Guangwei. Parameter Identification of Active Magnetic-Rotor System Based on Model Updating Using Complex Mode and Frequency Response Function. [Masters Thesis]. Nanjing; Nanjing university of Aeronautics and Astronautics, 2010.

[34] Sinha P. K. Electromagnetic Suspension: Dynamics and Control. London, P.Pergrinus U.K.,1987,290.

[35] Mohamed A. M. Busch-Vishniac I. Imbalance Compensation and Automation Balancing in Magnetic Bearing Systems Using the Q Parameterization Theory. IEEE Transactions on Control System Technology, 1995.3(2):202-211.

[36] Nonami K. T., Ito. μ Synthesis of Flexible Rotor-Magnetic Bearing Systems. IEEE Transactions on Control System Technology.1996, 4(5):503-512.

[37] Lun K. Y., Coppola V. T. Adaptive Auto Centering Control For an Active Magnetic Bearing Supporting A Rotor With Unknown Mass Imbalance. IEEE Transactions on Control System Technology.1996, 4(5): 587-597.

[38] Shiau T. N., Sheu G. J. Vibration & Control of A Flexible Rotor in Magnetic Bearings Using Hybrid Method & H Control Theory. Journal of Engineering For Gas, Turbine & Power. 1997,119:179-195.

[39] Komori M., Kumamoto M. A Hybrid-Type Superconducting Magnetic Bearing System with Nonlinear Control. IEEE Transactions on Applied Superconductivit y. 1998, 8(2): 79-83.

[40] Hajjaji A. E., Ouladsine M. Modeling and Nonlinear Control of Magnetic Levitation Systems. IEEE Transactions on Industrial Electronics.2001, 48(4):831-838.

[41] Nicholas J.C., Whalen J.K., Franklin S.D. Improving Critical Speed Calculation Using Flexible Bearing Support FRF Compliance Data. N.Y., USA ,Dresser-Rand Wellsville, 2002.

[42] Okoro U. G., Xie ZhenYu, Guo Qintao. Influence of Metal Rubber Ring On the Dynamics of Complxed Bearing System for Optimum Performance. Proc. International Conference on Electrical Information and Control. Wuhan, 2011. accepted.

[43] Seto K. A New Modeling Technique and Control System Design of Flexible Rotor Using Active Magnetic Bearing for Motion and Vibration Control. Proc. of the 9th International Symposium on Magnetic Bearings, CD-ROM, 2004.

[44] Seto K.Levitation and Vibration control of a Flexible rotor by using active magnetic bearing. Proc. 11th International Symposium on Magnetic Bearings.Japan,2008.

Acknowledgement

Acknowlegement goes to God Almighty, the source of my strength and inspiration.

I would like to acknowledge the contributions of my indefatigable supervisors; Xie ZhenYu and Guo Qintao, and all the teachers I passed through. I am grateful for your efforts.

I want to say a big thank you to the following colleagues at No. 6 building; Zhang Jingting, Guo Hua, MouWexing, Zhuang, Qing Cai, Zhang Suying and Wu Kaifeng. I wouldn't have done any better without your advices. Further thank you goes to all my colleagues at B331: Cai, Qing GuangWei, Zhang Jian, Kanji Chuen, Luipulin and Huang. Time flies when am with you guys.

Appreciation goes to the Association of Nigerians in Nanjing; to my President Oloche, Soledayo, Debbie, Salisu, to mention but a few. And to the Catholic cumminity in Nanjing; Fr. Anthony, Anthony, Marvin, Loretta, Kibaroya, Pamela etc, I say "thank you for all your prayers and moral supports". God bless you all.

This appreciation would not be complete without recognition of the following God-sent friends; Julin, Tina, Apple, Juana, Sun, Xiaoshueyi, Ojeide and my roommate Chiko. You are the best.

To the members of my family; Mr & Mrs V. O. Okoro, Chinedu, Kelechi, Okechukwu, Ezinne, Ugochukwu and Chioma, I say "The Lord is good … all the time".

Finally, to Megg because, she is for me.

Publications

Publications

1. Okoro U.G., Xie ZhenYu, Guo Qintao. Influence of metal rubber ring on the dynamics of metal rubber system for optimum performance. Proc. International Conference on Electrical Information and Control, Wuhan, 2011.(*accepted*)

Research Subject

2. National Nature Science Foundation of China, “Research on dynamic characteristics of flexible rotor supported on Active Magnetic Bearing” (No. 50675105)